

UNIVERSITY OF MIAMI SEA GRANT PROGRAM

CIRCULATING COPY
Sea Grant Depository

(Ocean Engineering)

(Ocean Engineering)

The Effects of Tilt on a Savonius Rotor Exposed to a Turbulent Flow Regime

HOWARD C. SERKIN

CIRCULATING COPY
Sea Grant Depository

Sea Grant Technical Bulletin #25

The Effects of Tilt on a Savónius Rotor Exposed to a Turbulent
Flow Regime

Howard C. Serkin

University of Miami Sea Grant Program - NOAA Sea Grant No. 2-35147

Coral Gables, Florida 1972

The research presented in this bulletin was submitted as a thesis in partial fulfillment of the requirements for the degree of Master of Science

Price: \$3.00

Library of Congress Catalog Card Number: 72-97692

The University of Miami's Sea Grant Program is a part of the National Sea Grant Program, which is maintained by the National Oceanic and Atmospheric Administration of the U. S. Department of Commerce.

Information Services
Sea Grant Institutional Program
University of Miami
Box 9178
Coral Gables, Florida 33124

PREFACE

The Sea Grant Colleges Program was created in 1966 to stimulate research, instruction, and extension of knowledge of marine resources of the United States. In 1969, the Sea Grant Program was established at the University of Miami.

The outstanding success of the Land Grant Colleges Program, which in 100 years has brought the United States to its current superior position in agricultural production, helped initiate the Sea Grant concept. This concept has three primary objectives: to promote excellence in education and training, research, and information services in sea related university activities including science, law, social science, engineering and business faculties. The successful accomplishment of these objectives, it is believed, will result in practical contribution to marine oriented industries and government and will, in addition, protect and preserve the environment for the benefit of all.

With these objectives, this series of Sea Grant Technical Bulletins is intended to convey useful studies quickly to the marine communities interested in resource development without awaiting more formal publication.

While the responsibility for administration of the Sea Grant Program rests with the National Oceanic and Atmospheric Administration of the Department of Commerce, the responsibility for financing the Program is shared by Federal, industrial and University contribution. This study, The Effects of Tilt on a Savonius Rotor Exposed to a Turbulent Flow Regime, is published as a part of the Sea Grant Program and was made possible by Sea Grant projects in Ocean Engineering Education.

TABLE OF CONTENTS

	PAGE
CHAPTER I	
INTRODUCTION.....	1
CHAPTER II	
BACKGROUND.....	7
CHAPTER III	
EXPERIMENTAL DESIGN.....	11
CHAPTER IV	
INSTRUMENTATION.....	24
CHAPTER V	
INCLINOMETER.....	33
CHAPTER VI	
DATA SUMMARY AND ANALYSIS.....	42
CHAPTER VII	
CONCLUSIONS AND RECOMMENDATIONS.....	59
BIBLIOGRAPHY.....	63

LIST OF FIGURES

FIGURE	PAGE
1. Principle of Current Profiling Method Used in the Florida Current.....	2
2. Principle of New Current Profiling Method.....	3
3. Current Profiler on Deck.....	5
4. Current Profiler on Mooring Cable.....	6
5. Instrument Test Fixture.....	13
6. Spherical and Cylindrical Pressure Vessels.....	14
7. Cylindrical Instrument Package in Test Fixture.....	15
8. Spherical Instrument Package in Test Fixture.....	16
9. Experimental Setup.....	18
10. Mixing Pattern of Round Jet Entering Stationary Fluid.....	21
11. The Aanderaa Recording Current Meter, Model 4.....	25
12. Oscilloscope Trace of Data Pulse Train.....	27
13. Data Decoding System.....	28
14. Block Diagram of Data Decoding and Processing System.....	29
15. Block Diagram of Digital Interface.....	30
16. Spherical Instrument Package.....	31
17. Pendulum Displacement Sensor.....	36
18. Exploded View of Inclinator.....	38
19. Inclinator in Spherical Instrument Package.....	41
20. Influence of Tilt on Rotor Output.....	49
21. Influence of Tilt on Cylindrical Instrument Package.....	51

LIST OF FIGURES

FIGURE	PAGE
22. Influence of Tilt on Spherical Instrument Package.....	52
23. Influence of Tilt on Cylindrical and Spherical Instrument Packages.....	56
24. Comparison of Unhoused Rotor and Cylindrical Instrument Package.....	57
25. Comparison of Unhoused Rotor and Spherical Instrument Package.....	58

LIST OF TABLES

TABLE	PAGE
1. Data Format of Current Velocity Measurement Print-Out.....	43
2. Summarized Data from Inclination of Cylindrical Instrument Package.....	46
3. Summarized Data from Inclination of Spherical Instrument Package.....	47

CHAPTER I

INTRODUCTION

There is a river in the ocean. In the severest droughts it never fails, and in the mightiest floods it never overflows. Its banks and its bottoms are of cold water, while its current is of warm. The Gulf of Mexico is its fountain, and its mouth is the Arctic Seas. It is the Gulf Stream. There is in the world no other such majestic flow of waters. Its current is more rapid than the Mississippi or the Amazon, and its volume more than a thousand times greater (Maury, 1858).

The Division of Physical Oceanography at the University of Miami Rosenstiel School of Marine and Atmospheric Science has developed a method for obtaining high resolution current profiles in the Gulf Stream (Düing and Johnson, 1972). This method measures currents in regions with moderate and strong flows. A new method is currently being developed that will provide finer detail in the vertical structure of currents and extend the capability of the profiling system to include regions with weak flows (Van Leer and Düing, 1972).

The principle utilized in the profiling system developed by Düing and Johnson is shown in figure 1. The profiler consists of a self-contained Aanderaa current meter attached to a cylindrical hull (Aanderaa, 1964; Dahl, 1969). The instrument package is attached by a roller to a taut wire suspended beneath the anchored vessel and slowly descends through the water column.

The principle utilized in the new profiling system developed by Van Leer and Düing is shown in figure 2. The profiler, shown in

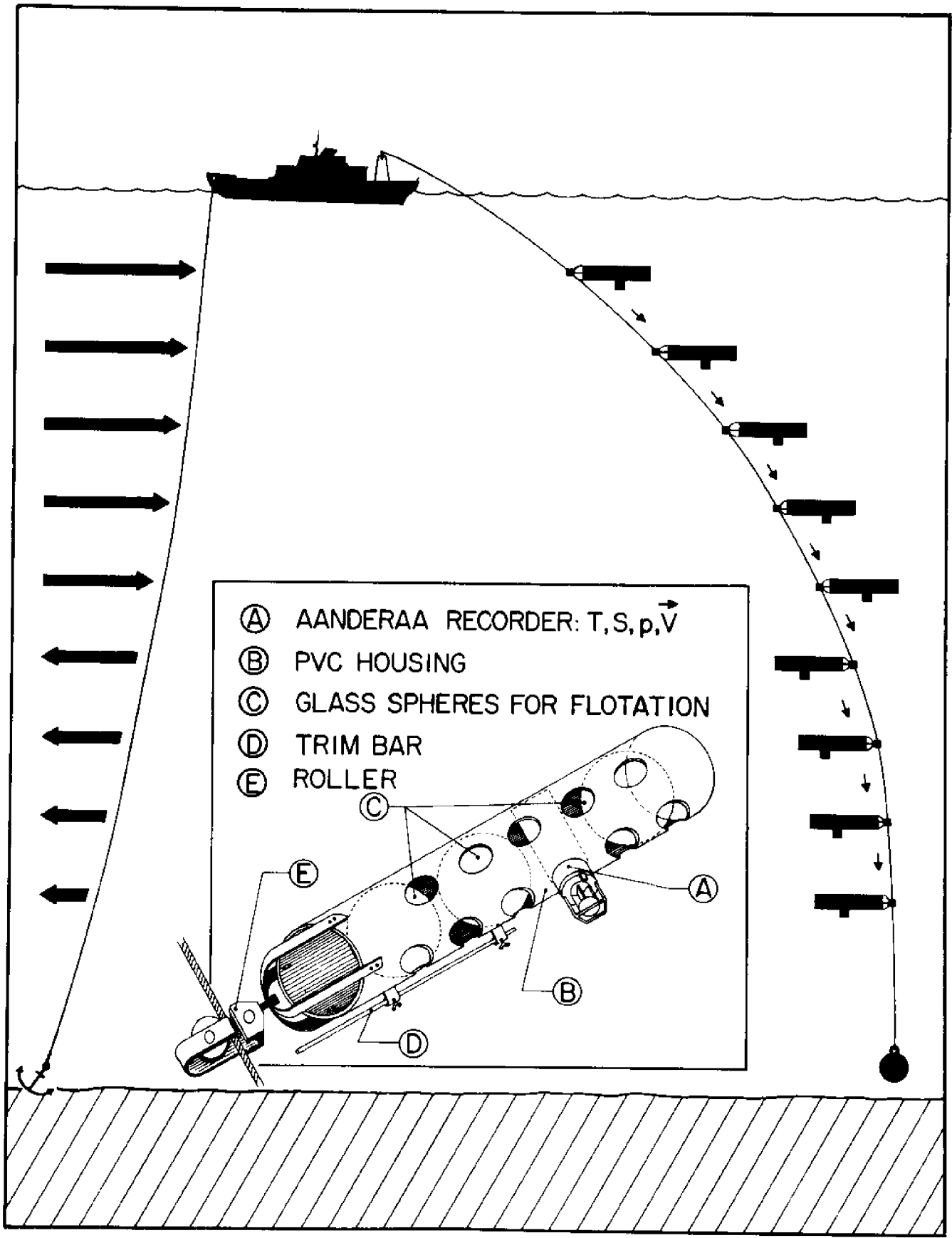


Figure 1. Principle of current profiling method used in the Florida Current.

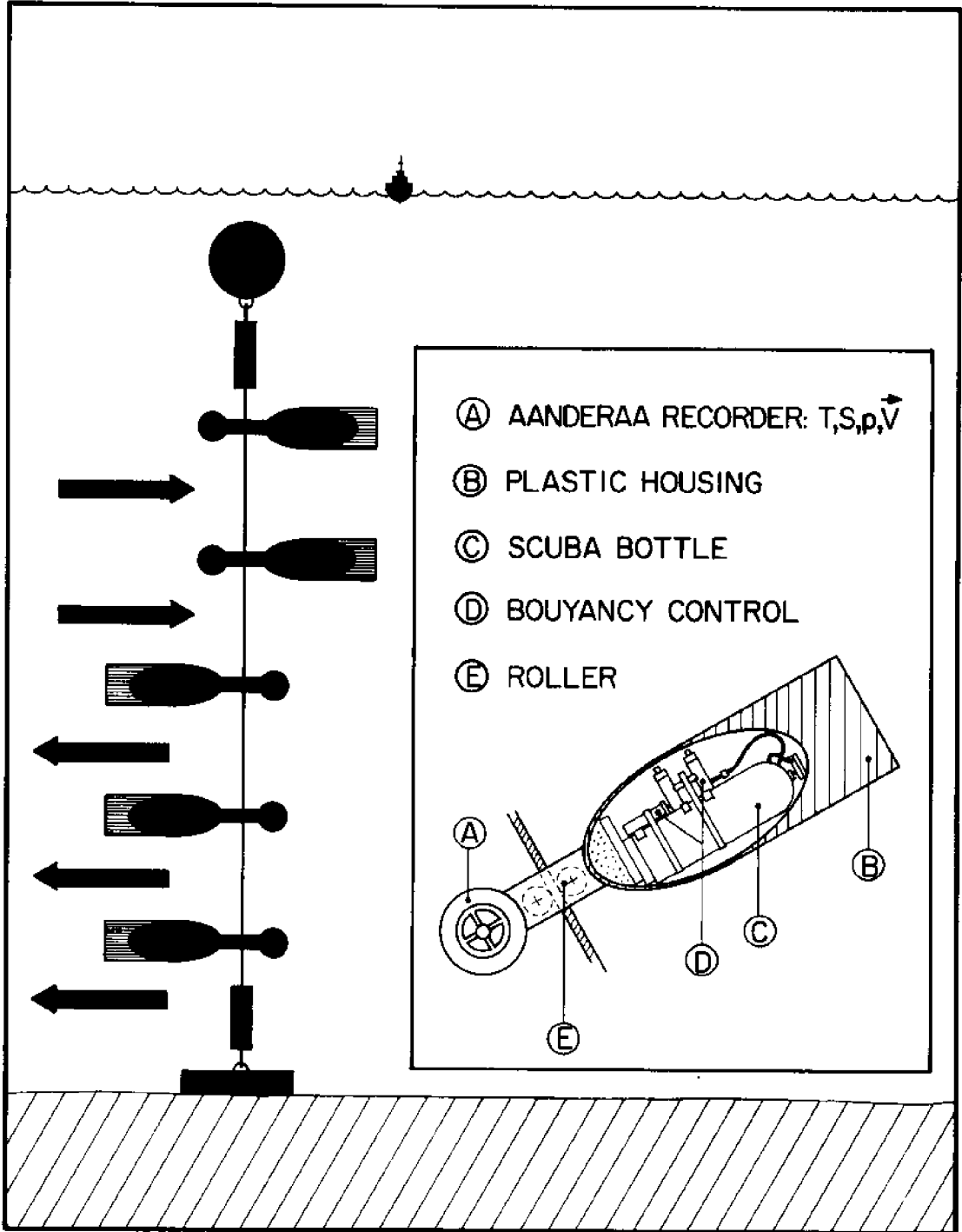


Figure 2. Principle of new current profiling method.

figures 3 and 4, consists of three major components: the instrument package, the roller block, and the buoyancy control mechanism. The instrument package is a metal sphere housing a repackaged Aanderaa current meter. The current speed sensor is a Savonius rotor mounted with its axis parallel to the profiler's pitch axis. The large roller block guides the profiler as it traverses the water column and attempts to decouple the profiler from the motions and vibrations of the mooring cable. The buoyancy control mechanism regulates the density of the profiler as it traverses the water column between the preset upper and lower depth settings. The hydrodynamic design of the plastic housing maintains the instrument package's orientation into the current flow.

While designed to profile the water column in a horizontal orientation, internal and external forces act to displace the profilers from their designed horizontal axis and introduce errors into their measurement of current velocity.

The necessity for determining the occurrence and magnitude of these errors prompted this investigation into the effects of tilt on a Savonius rotor exposed to a turbulent flow regime and the development of an instrument to measure rotor inclination.

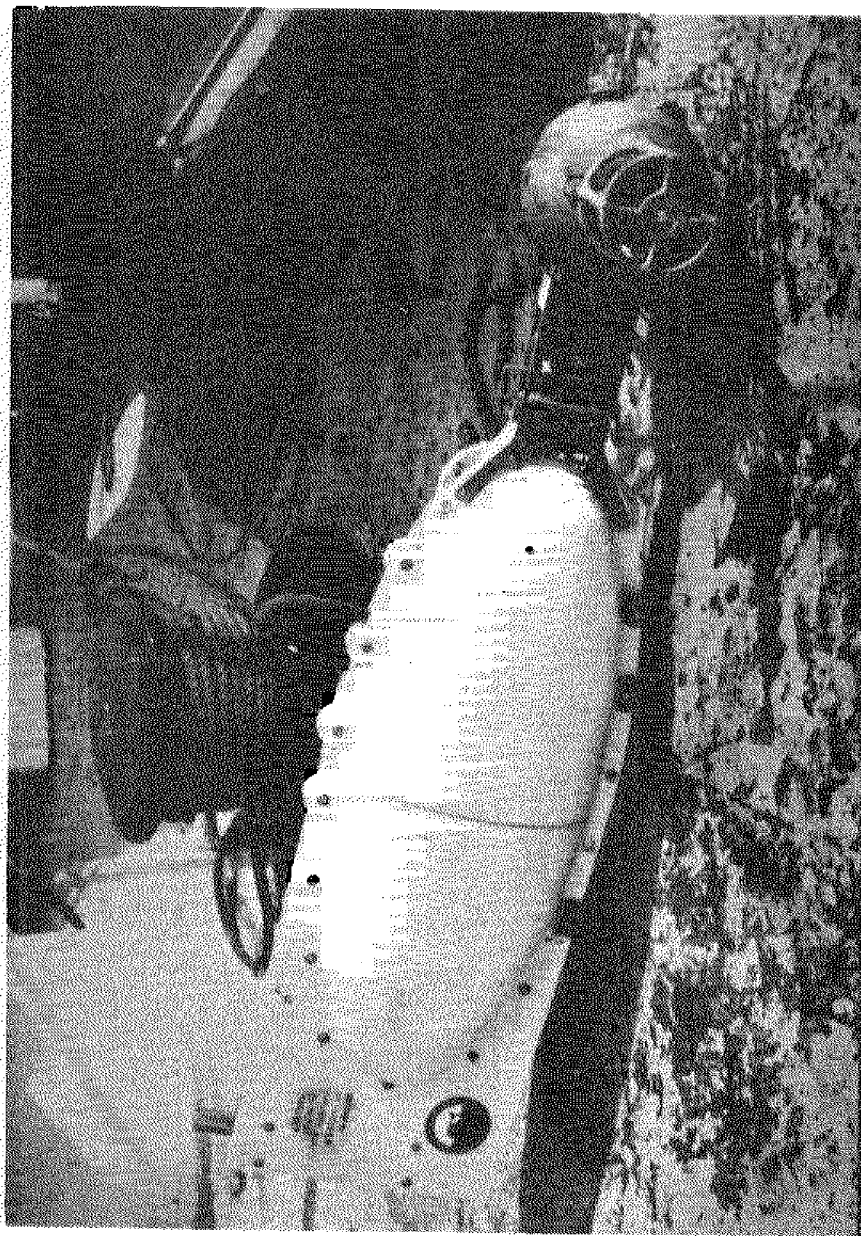


Figure 3. Current profiler on deck.



Figure 4. Current profiler on mooring cable.

CHAPTER II

BACKGROUND

In recent years, the Savonius rotor current meter has undergone an accelerated acceptance and usage by the oceanographic and limnographic communities as a versatile, durable, and relatively inexpensive current speed sensor. S. J. Savonius' original experiments with the "wing rotor" were conducted to develop a technique to efficiently harness the power of the wind (Savonius, 1925). Savonius found that there were a large number of mechanical applications compatible with his rotor. One of these applications was the use of the "wing rotor" for an oceanographic current meter (Savonius, 1931).

Difficulties involving rotor stall points and variability in angular rates of rotation of the Savonius rotor current meter plagued early experimenters. The problems were somewhat reduced with the development of the double tier rotor with one pair of vanes rotated 90° with respect to the other pair. This configuration, which utilized two inch radius half cylinder vanes and a flow passage width of two inches, responded well at and above 0.005 knots and did not appear to respond to velocity components parallel to the vertical axis of revolution (Snodgrass, 1955; Gaul, 1962b).

Since the first successful development and introduction of the Savonius rotor current meter by Mr. James M. Snodgrass of Scripps Institution of Oceanography, oceanographers and ocean engineers have been concerned about its operating characteristics and the interpretation

of the data it has provided.

One of the principal investigators into the problems of calibration and performance characteristics of the Savonius rotor current meter is Dr. Roy D. Gaul, presently associated with the Office of Naval Research. Dr. Gaul conducted extensive experiments with the Savonius rotor and provided information essential to the proper interpretation of the data generated by Savonius rotor current meters (Gaul, 1962a; Gaul, 1962b; Gaul, 1963; Gaul, Snodgrass, Cretzler, 1963).

A significant characteristic of the Savonius rotor is that it rotates at a higher revolution rate in the natural wind than it does in the wind tunnel. Gaul (1962b) attributes this characteristic to the omnidirectional nature of the rotor such that it utilizes energy of all horizontal components of flow within its response spectrum and that the spectrum of turbulence associated with the mean fluid motion will be reflected in rotor output. Savonius (1931) found that as compared to an optimum speed ratio of 0.85 in the wind tunnel, there is an optimum speed ratio of 0.92 - 1.00 in the natural wind. The optimum speed ratio is the highest value for the ratio of vane tip speed to wind speed at a load giving most efficient power output.

This difference in rotation rate between the natural wind (natural current) and the wind tunnel (tow tank) environment is of great importance to the engineer or scientist analyzing field data collected by a Savonius rotor transducer. The studies carried out to date on the response characteristics of the Savonius rotor have been performed in a tow tank environment. Addressing this problem, Gaul (1962b) points out:

There are many difficult aspects of precision of calibration in the low speed range..."Cali-

bration precision" will herein be construed to mean the absolute accuracy with which results may be consistently reproduced under controlled conditions in the tow tank. That this may be significantly different from precision of measurements in the field follows from the previously mentioned conclusions of Savonius (1931) related to more efficient rotor performance in natural wind than in a wind tunnel. This difference is probably accentuated by the presently accepted practice of towing the instrument through still water since the goal is complete suppression of turbulence whereas the air moving through a wind tunnel is mainly limited in scale of turbulence...Why, then, has a procedure not been adopted whereby the meter is rigidly suspended in turbulent flow? One answer is simply that suitable facilities and the time to use them have not been readily available. More important, however, is that "turbulent flow" is by comparison much more difficult to control and measure than "still water"...Considerable investigation of rotor properties under various conditions of turbulent flow is in order.

The rotor serving as the current speed sensor in the University of Miami's current profiling system will experience both tilt with respect to its vertical axis and a turbulent flow regime as it traverses the water column in its open ocean data collection mode. While limited tow tank data are available on the effect of tilt on certain rotor and housing configurations, the author undertook this experiment to specifically identify the errors introduced as the Aanderaa rotor and housing configurations are inclined into and away from a horizontal turbulent current. The four objectives of this study are:

1. Determine and plot the curve of relative rotation ratio versus angle of tilt (in a turbulent horizontal flow pattern) for the Aanderaa model 4 current meter used by Düing and Johnson in their high resolution current profiling experiments in the Straits of Florida

(Düing and Johnson, 1972).

2. Determine and plot the curve of relative rotation ratio versus angle of tilt (in a turbulent horizontal flow pattern) for the repackaged recording current meter presently in use by Van Leer and Düing in their unattended profiling system (Van Leer and Düing, 1972).

3. Compare the data collected in this study with the observations obtained by other investigators analyzing the effects of tilt on a Savonius rotor exposed to a non-turbulent (or turbulent suppressed) flow regime.

4. Develop an instrument to detect the occurrence, magnitude, and direction of rotor inclination.

CHAPTER III
EXPERIMENTAL DESIGN

Turbulence is the random irregular motion of fluid particles in time and space. One of the most difficult problems in an experiment of this nature is that of describing the turbulent flow pattern. This problem is made more important by the fact that rotor response is different to various scales of turbulence.

In the turbulent flow of a fluid, perturbations in the local velocity result in the transporting of fluid in all directions throughout the body of fluid considered moving in some pattern of average flow. In the discussion of turbulent flow, the velocity vector is usually separated into bulk or primary velocity components, upon which are superimposed secondary velocity components corresponding to the irregular, random motions. If u_i , v_i , and w_i are the instantaneous components in the x, y, and z directions of a steady flow velocity, \bar{V} , then

$$u_i = u + u'$$

$$v_i = v + v'$$

$$w_i = w + w'$$

where u , v , and w are the averages of bulk velocities and u' , v' , and w' are the superimposed fluctuating components. In the literature, the relative intensities of turbulence

$$\frac{\sqrt{(u')^2}}{u} \quad \text{and} \quad \frac{\sqrt{(v')^2}}{v} \quad \text{and} \quad \frac{\sqrt{(w')^2}}{w}$$

are quoted as percentages and serve as measures of turbulence. Because the fluctuating components are usually small, and because at any fixed point in space the velocity components vary rapidly in magnitudes, special instrumentation, such as hot wire anemometers, must be used for these measurements (Shepherd, 1965).

Although the above approach leads to a statistical theory that yields some information on turbulence, the phenomenological approach has to date been more valuable in producing relationships for quantitative use with turbulent flows (Shepherd, 1965).

Taking the phenomenological approach, the author designed this experiment to parallel a well documented experiment performed by Forstall and Gaylord (1955) which described the turbulence associated with a submerged water jet.

An instrument test fixture (figure 5) was designed and built to rigidly support both the cylindrical and spherical instrument housings during the data collection phase of the experiment (figures 6, 7, and 8). The test fixture was manufactured from 0.250 inch aluminum. The center bracket assembly can be rotated through $+90^\circ$ and locked in place at multiples of 11° by tightening the two end wing nuts and the locking set screw. The following tilt positions were utilized for this study: -33° , -22° , -11° , 0° , $+11^\circ$, $+22^\circ$, and $+33^\circ$. A removable center bracket insert supports the cylindrical instrument housing during its test phase and is removed for the spherical housing. The high concentration of mass in the base and legs provide a low center of gravity for the fixture, thus insuring stability when the housings are in place. The wide spacing of the legs provides resistance to the upsetting moment created by the drag force which the current flow induces on the instrument packages.

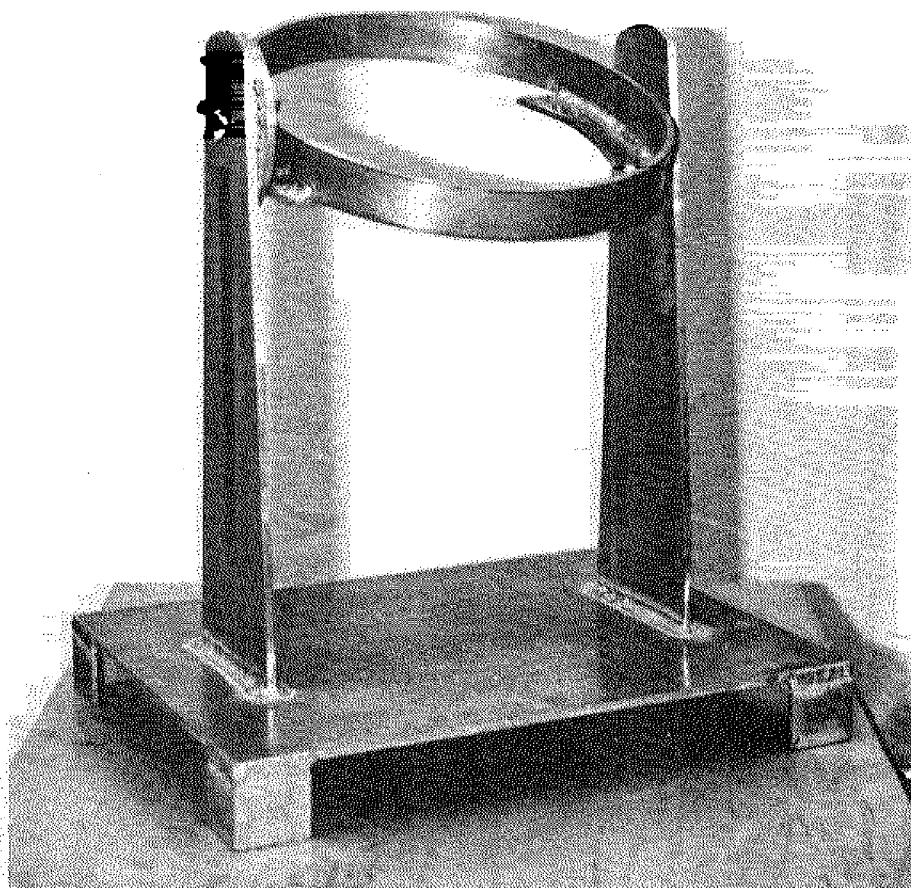


Figure 5. Instrument test fixture.

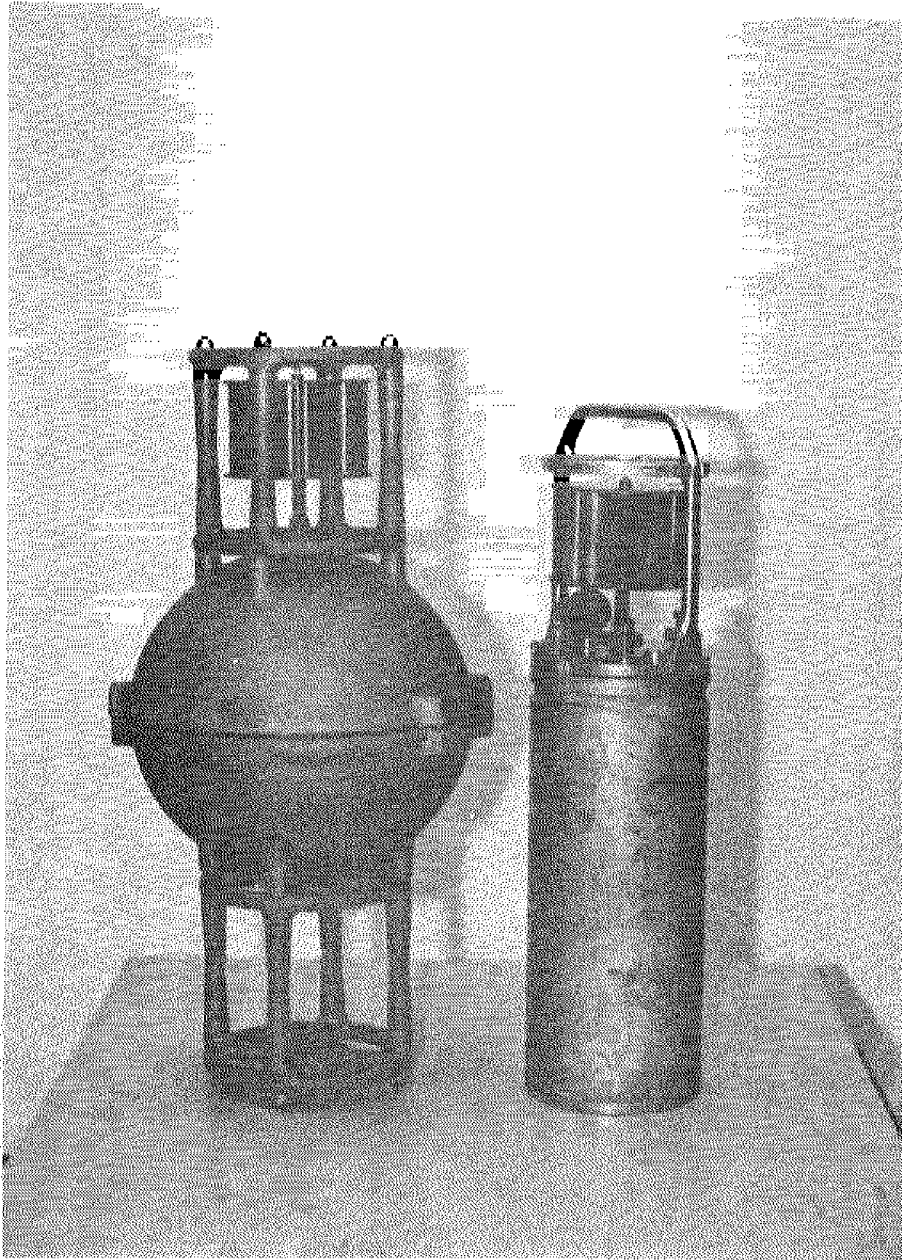


Figure 6. Spherical and cylindrical pressure vessels.

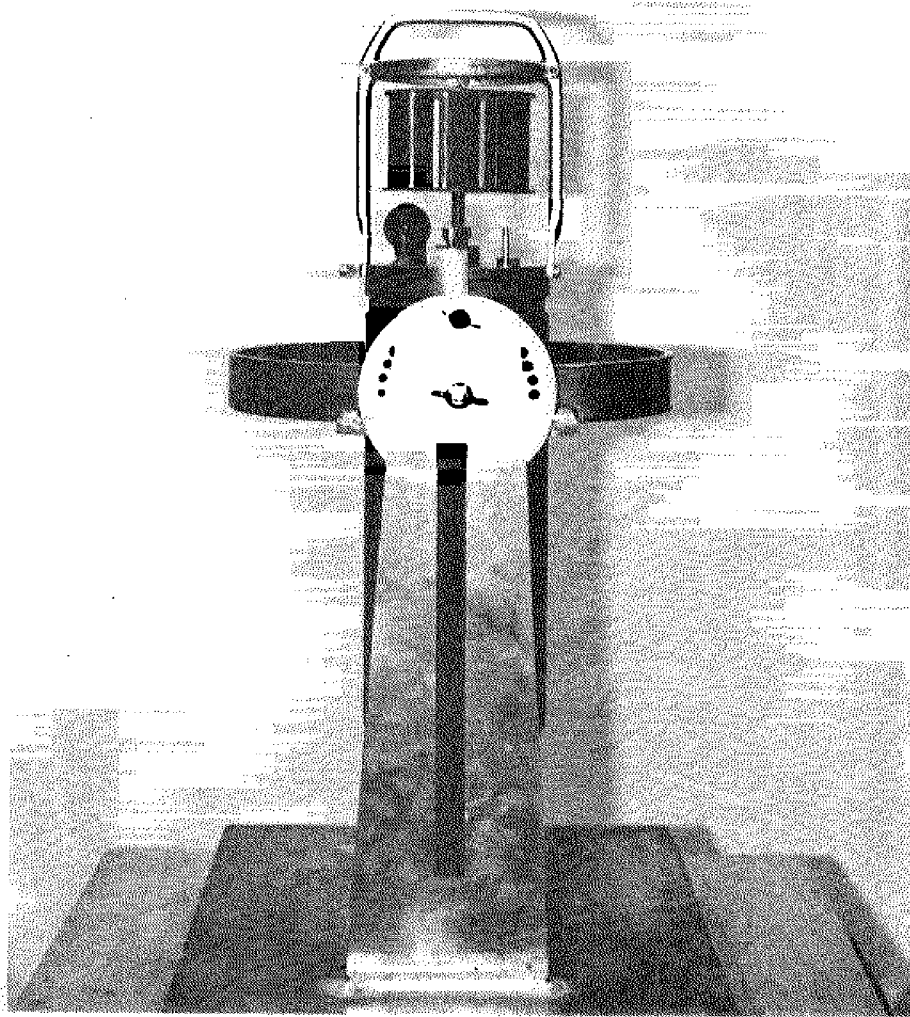


Figure 7. Cylindrical instrument package in test fixture.

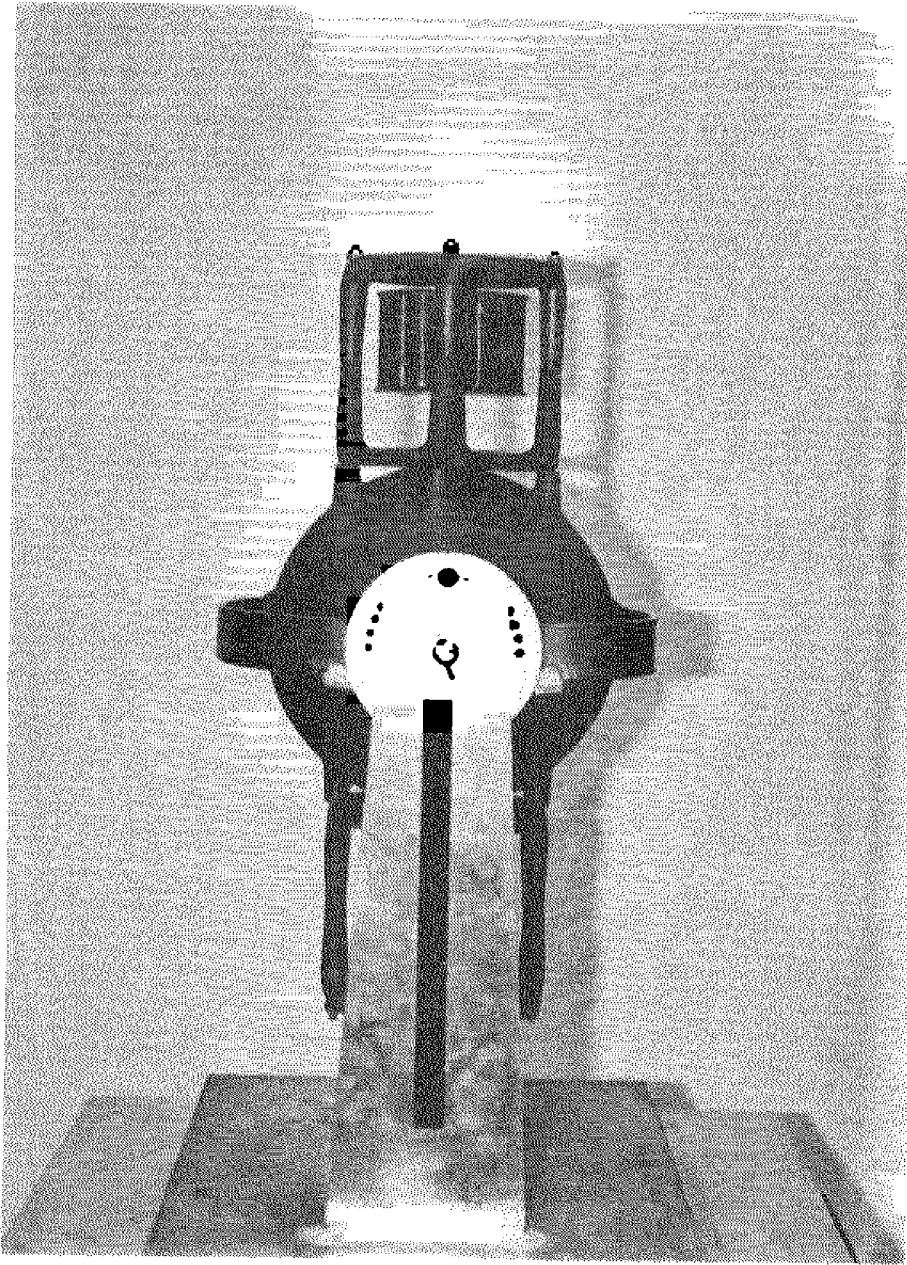


Figure 8. Spherical instrument package in test fixture.

Figure 9 shows the experimental set up. The study was conducted in a 40 x 20 x 8 foot concrete swimming pool. Where the measurements were collected ($Z > 5$ feet), there was no evidence of any disturbance caused by the air-water interface at the surface of the pool. The air temperature was 27°C and the fresh water temperature was 23°C . The experimental site was enclosed by a fine mesh screen which prevented capillary waves (period < 0.1 sec) from forming.

A one inch hose was connected to the discharge outlet of a centrifugal pump in the pool's filter system. The hose was supported in an adjustable tripod that allowed the hose to be moved in the vertical and horizontal directions. This adjustment feature was needed to insure that the axis of current flow was always directed at the geometric center of the rotor and that a constant distance was maintained between the hose nozzle and the geometric center of the rotor through all inclinations.

A Bendix model S-6b ducted current sensor with a deck readout meter was used to survey the imposed velocity profile in order to establish the distance the nozzle should be from the rotor. Two experimental constraints had to be satisfied. First, the velocity of the horizontal current had to be approximately 0.80 knots. This requirement was established so that a comparison between the data collected during this experiment and that collected by Gaul at 0.74 knots could be made. Second, the velocity profile across the rotor had to be uniform. Within the accuracy of the ducted current meter (± 0.06 knots), the velocity profile had to be constant over an area twice as large as the longest dimension of the rotor (rotor width, 4.125 inches).

A distance of 48 inches between nozzle and rotor satisfied both

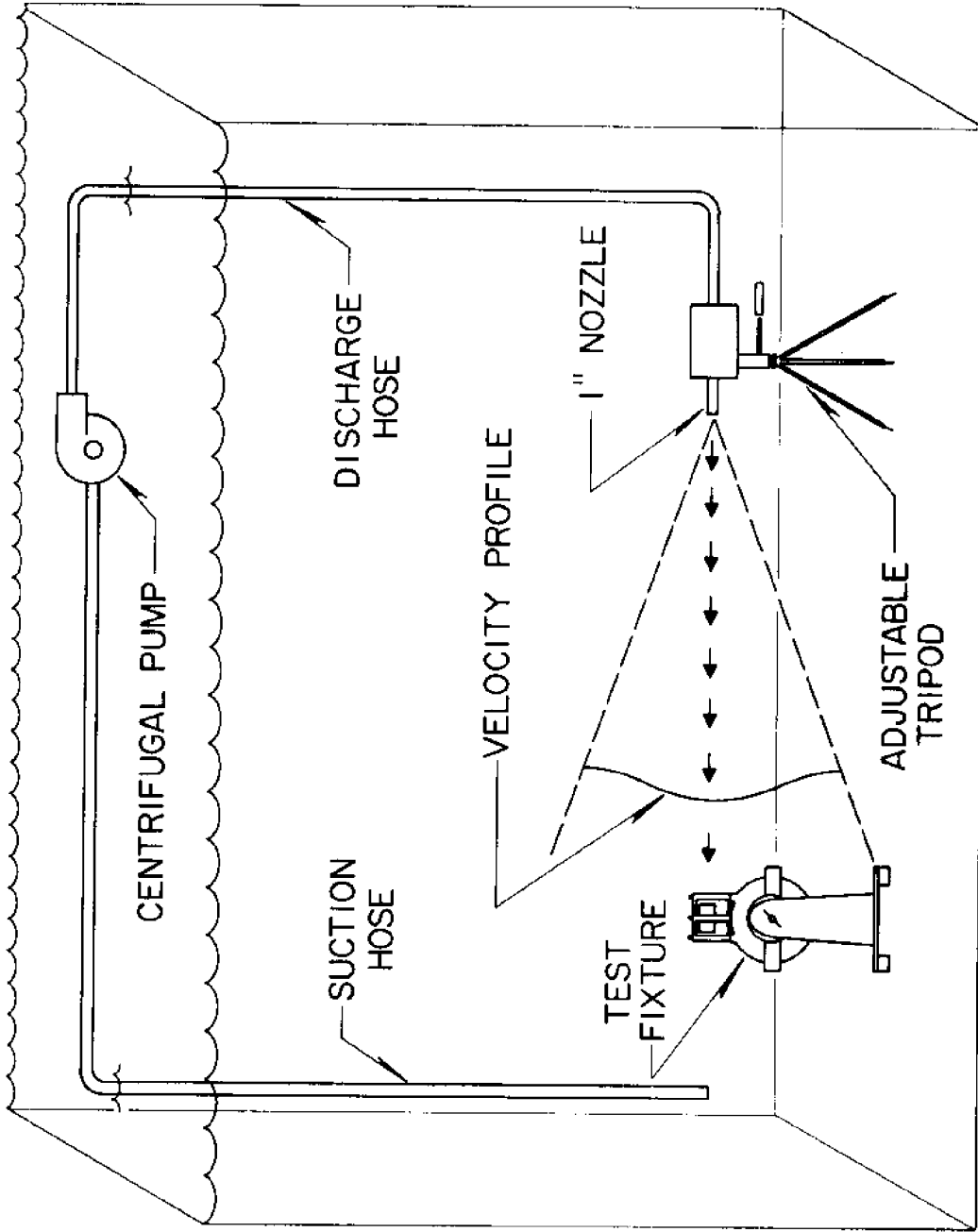


Figure 9. Experimental setup.

constraints. The current speed impinging upon the rotor was 0.80 knots and the velocity profile was constant over a nine inch diameter circle. While the current velocity was uniform across the entire rotor, the velocity profile impinging upon the instrument housings was not uniform. The expected decrease in velocity with increasing distance from the flow axis was observed. This fact is considered by the author to be a major limitation in the experimental design and will be further discussed with the conclusions and recommendations.

The cylindrical and spherical instrument packages were tilted into and out of the imposed current at 11° increments. The rotor rotation rate was measured at each position for about five minutes and the sampling interval was five seconds. The tilt angle, θ , was taken as positive when the leading edge of the rotor was tilted up from the flow axis and negative when the leading edge was down. This sign convention was adopted to conform with the terminology used by Gaul (1963) in his tilt experiments.

Forstall and Gaylord indicate that whereas molecular diffusion is a characteristic of the fluid involved, turbulent diffusion is determined by the nature of the turbulence and for the same turbulence is independent of the fluid. Molecular diffusivity can be measured for each one of numerous fluids. In contrast, the relating of turbulent diffusion to various flow patterns is still a formidable problem and the solution to this problem is being investigated by several different methods. In the interim, many investigators have measured turbulent diffusion in simple geometries of flow and correlated the results by empirical formulations.

Of primary importance in the jet-diffusion problem are the trans-

port of material, temperature, and momentum. Forstall and Gaylord report the results of measurements of material and momentum diffusion in a submerged water jet. The jet (primary stream) is of circular cross section and when entering a stationary body of water (secondary) produces the mixing pattern shown schematically in figure 10.

The normal probability or error curve approximates the velocity profile of a circular jet. This fact has been shown by many investigators and was confirmed by Forstall and Gaylord. The relative rate of turbulent-material diffusion compared with turbulent-momentum diffusion is expressed as the turbulent Schmidt number and serves as a measure of turbulence. The normal probability curve presents a special convenience in the evaluation of turbulent Schmidt numbers from diffusion measurements. Velocity and concentration profiles in terms of the error curve are

$$\frac{u}{u_c} = \exp \left[-0.694 \left(\frac{r}{r_{mu}} \right)^2 \right]$$

where $\frac{\xi}{\xi_c} = \exp \left[-0.694 \left(\frac{r}{r_{m\xi}} \right)^2 \right]$

u = axial component of velocity

ξ = concentration of a tracer material per unit volume

r = radial distance from jet axis

r_{mu} = value of r for which $u = u_c/2$

$r_{m\xi}$ = value of r for which $\xi = \xi_c/2$

subscript c = values at $r = 0$

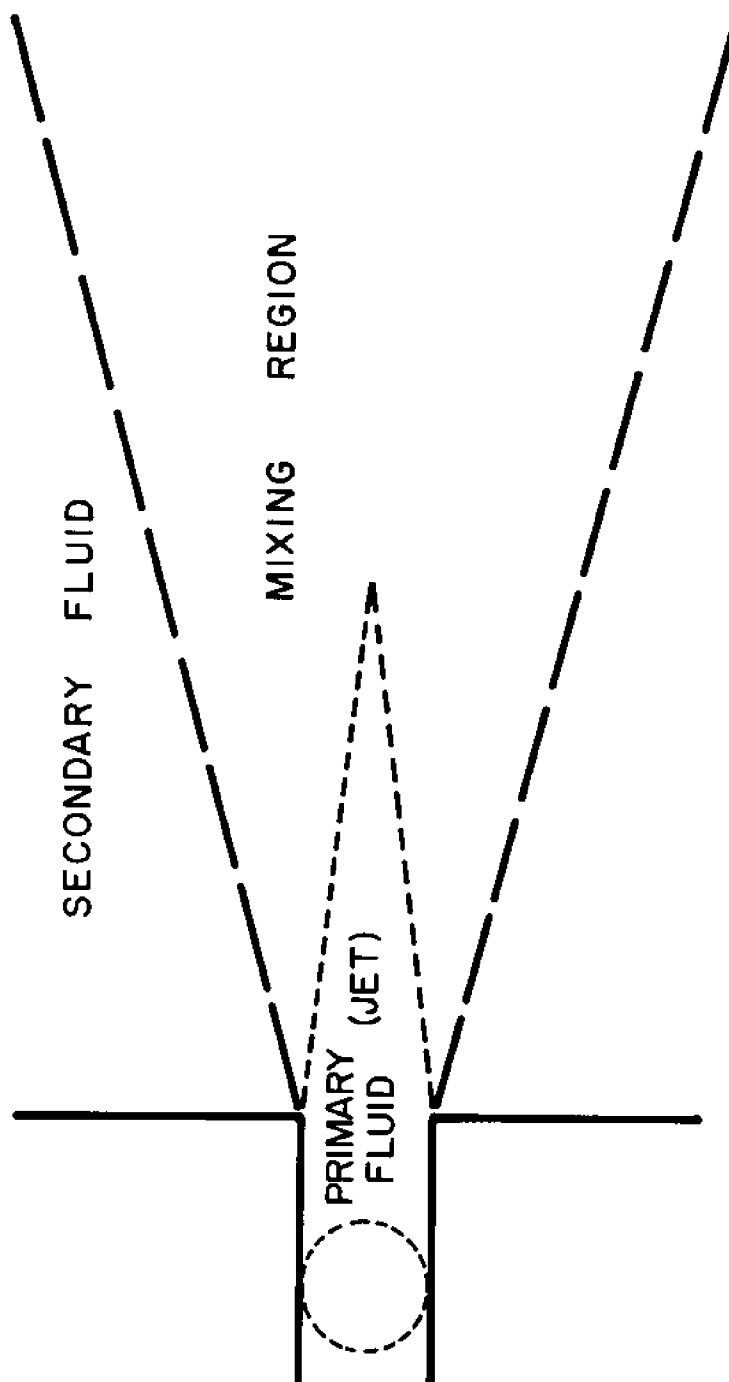


Figure 10. Mixing pattern of round jet entering stationary fluid.

This leads to

$$S \text{ (turbulent Schmidt number)} = \left(\frac{\tau_{mu}}{\tau_{m\xi}} \right)^2$$

Discharging from a 0.25 inch nozzle, Forstall and Gaylord found that at 30 nozzle diameters along the jet axis of flow the turbulent Schmidt number = 0.827. Forstall and Gaylord only measured values out to 32 nozzle diameters but because profile similarity is satisfied for both velocity and concentration, the same order of magnitude in the turbulent Schmidt number should be expected at 48 nozzle diameters.

The value of the Prandtl mixing length at 48 inches from the nozzle, according to the momentum-transport theory, is 0.816 inch. The value according to the modified vorticity-transport theory is 0.864 inch (Hinze, 1959).

Similarity and conservation of momentum and material flux result in equations for the jet axis values having the form

$$\frac{u_c}{u_0} = \frac{C_u D}{x}$$

$$\frac{\xi_c}{\xi_0} = \frac{C_\xi D}{x}$$

where

subscript 0 = value at $x = 0, r = 0$

x = distance from jet exit

C_u, C_ξ = empirical constants

D = jet diameter at $x = 0$

Forstall and Gaylord obtained $C_u = 6.4$ and $C_\xi = 5.2$. The author obtained $C_u = 6.6$. The difference between 6.4 and 6.6 is within the range of experimental error (Forstall and Gaylord, 1955).

The relative kurtosis between the Gaussian velocity profile observed in this experiment and that observed by Forstall and Gaylord remains to be examined. The velocity profile produced in this experiment was much flatter than that of Forstall and Gaylord. The reason for the difference is that the nozzle discharging into the test tank utilized by Forstall and Gaylord was flush with one wall of the tank. In this experiment, the nozzle was displaced from the tank wall which allowed the jet effect to pull additional masses of water into the main flow column and thus flatten the Gaussian velocity profile. This spreading out of the velocity profile was a positive effect in this experiment and provided a more uniform velocity profile across the rotor.

CHAPTER IV

INSTRUMENTATION

The Aanderaa model 4 recording current meter is a self-contained instrument used for recording the speed and direction of ocean currents, water temperature and conductivity, and instrument depth (see figure 11).

The instrument utilizes a rotor for the speed sensor, a magnetic compass for determination of direction, a thermistor for sensing temperature, a bourdon tube for depth measurement, and an induction coil for conductivity determination. An electro-mechanical encoder samples and converts the measurements into a 10 bit pulse-width modulated format which is serially recorded on 0.25 inch magnetic tape. A reference number and five data channels are recorded. The binary signals are also transmitted to the surface by means of a crystal controlled pulse coded acoustic carrier (16.4 KHz) thus permitting in situ monitoring. An internal quartz crystal clock, accurate to ± 2 sec/day over a temperature range of 0 to 20°C, actuates the instrument at regular intervals and the battery power supply provides energy for up to 12 months operation.

The motion of the velocity sensing rotor is transmitted through the pressure housing of the recording unit via a magnetic coupling. The rotor speed reduction ratio is 1200:1. The magnetic compass is housed inside the pressure housing. The velocity measurement is in integrated form, while the direction measurement is instantaneous.

The instrument measuring system consists of a rotary encoder mechanism

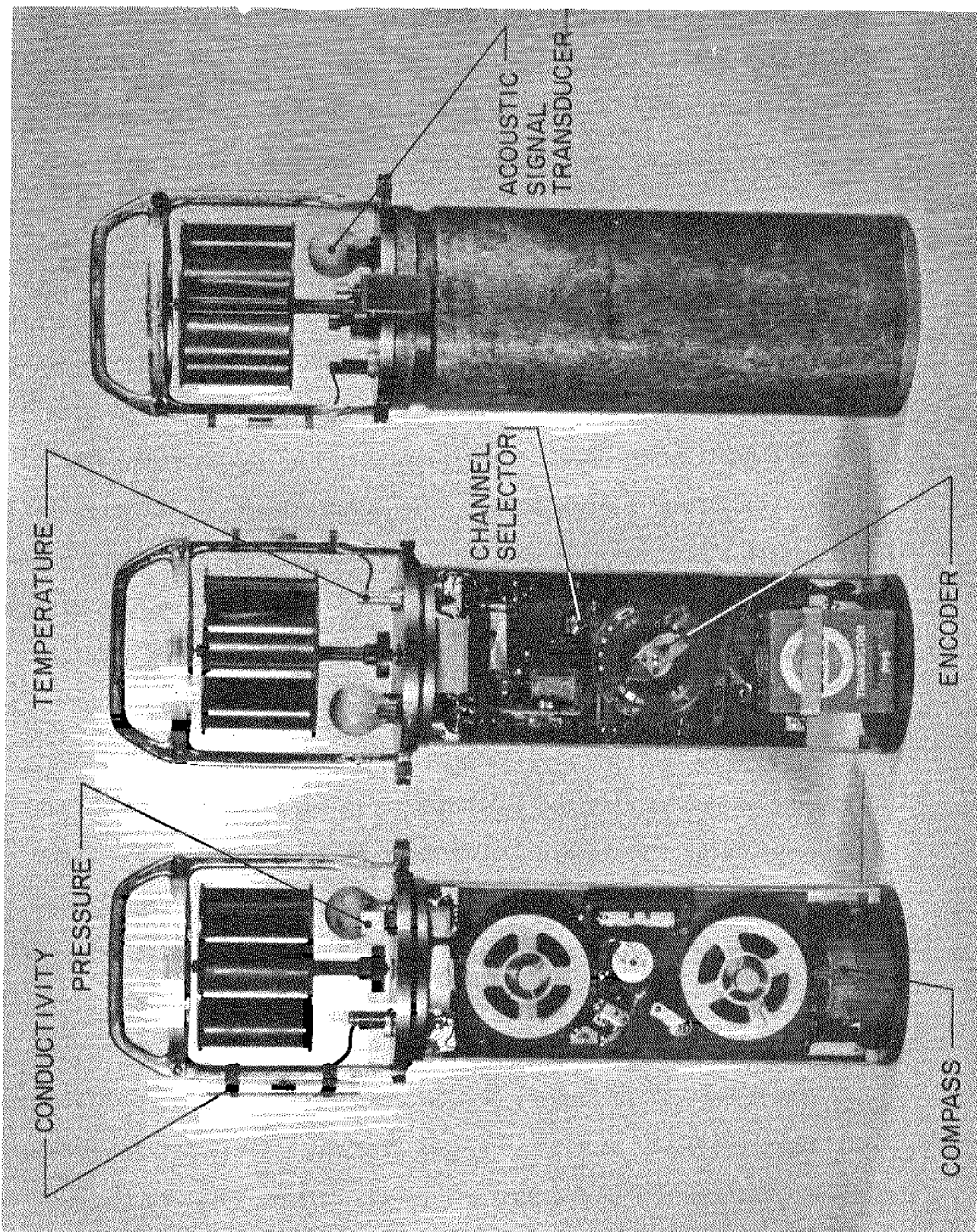


Figure 11. The Aanderaa Recording Current Meter, Model 4.

which sequentially measures six channels with a self-balancing bridge. The bridge gives a 10 bit word for each channel.

Aanderaa offers a mail service for tape reading. The service provides punched paper tape, industry compatible magnetic tape, direct print-out, or print-out in real values. Since delays of several weeks were experienced with the mail service, Mr. John Shearer, Research Assistant at the University of Miami, developed a decoding interface system which made the data immediately available (Shearer, 1972).

The computer interface system was designed to convert the data from the pulse-width coded binary format used by the current meter to an amplitude-coded binary format. The computer used has no provision for parallel data entry so the signal is serially fed into the A/D converter with a clock pulse signifying a bit. A program has been written to convert the data fed into a 4K Linc-8 minicomputer to an industry compatible format recorded on 7-track tape (Almeida, 1972).

Figure 12 shows an oscilloscope trace of the pulse train taken from the output terminal of a 2-track audio tape unit as a data tape is played back. The binary number shown is decimal 96. This output is fed into the computer interface. A photograph of the tape transport, interface, and computer is shown in figure 13. A block diagram of the system is given in figure 14 and a block diagram of the digital interface is shown in figure 15.

The spherical instrument package was developed by Dr. John Van Leer, Assistant Professor at the University of Miami. The spherical pressure vessel contains the same components as the current meter in the cylindrical pressure vessel. A modified configuration of component distribution was required to conform with the new shape (see figure 16). The current

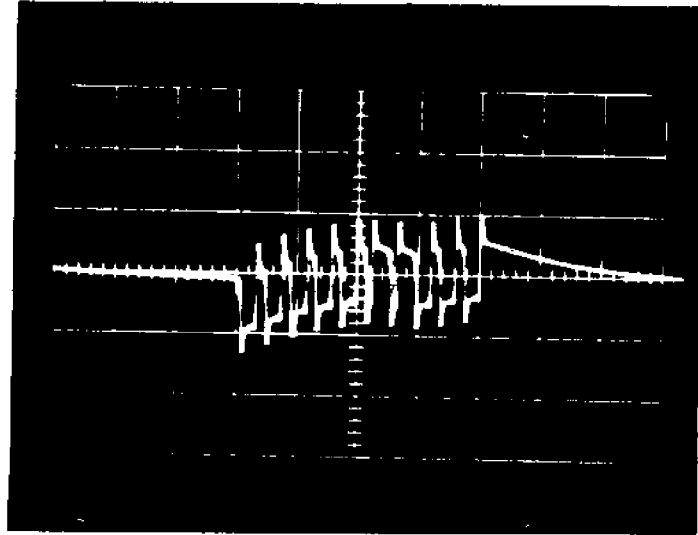


Figure 12. Oscilloscope trace of data pulse train.

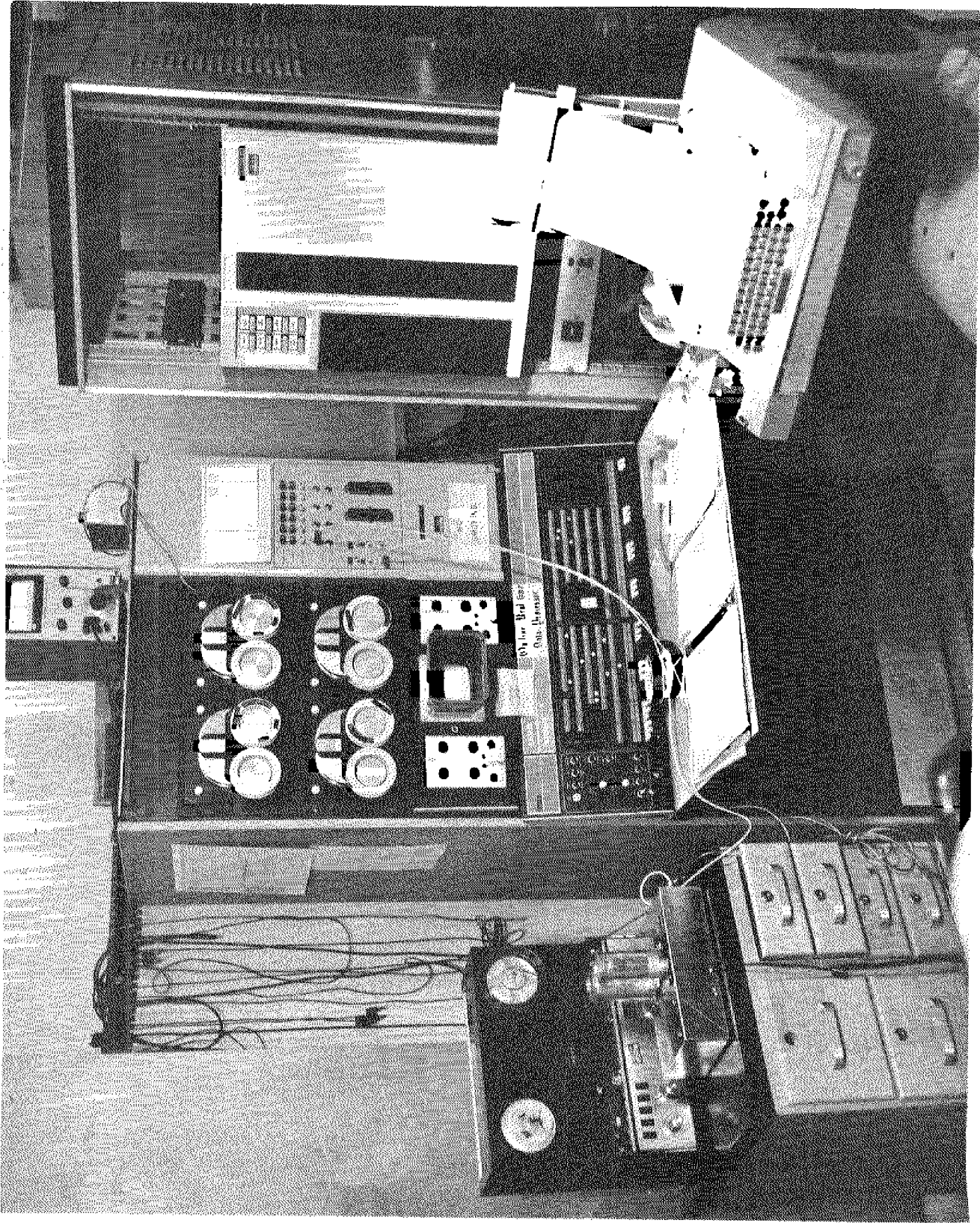


Figure 13. Data decoding system.

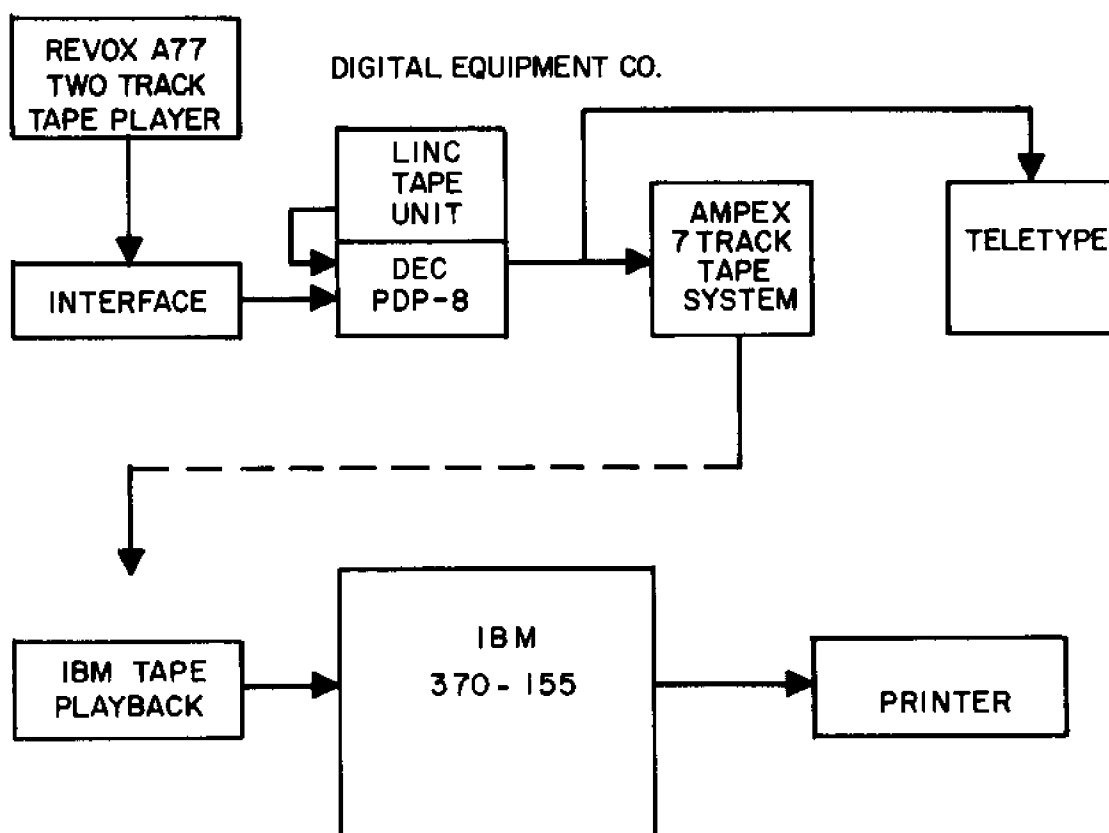


Figure 14. Block diagram of data decoding and processing system.

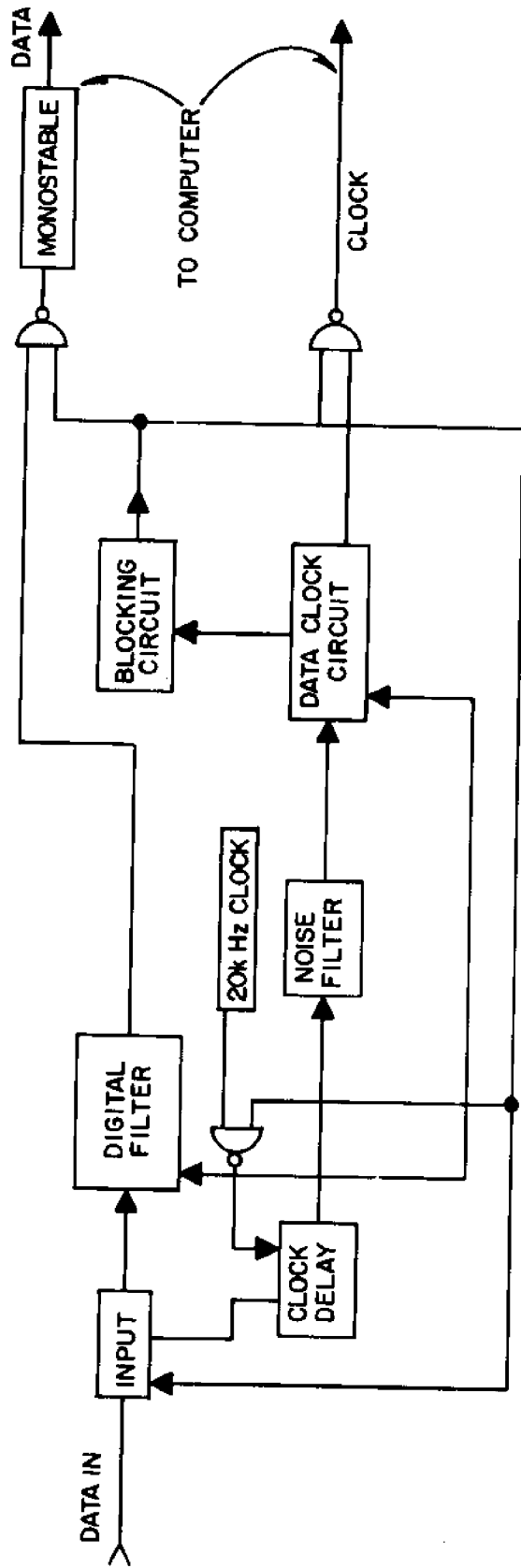


Figure 15. Block diagram of digital interface.

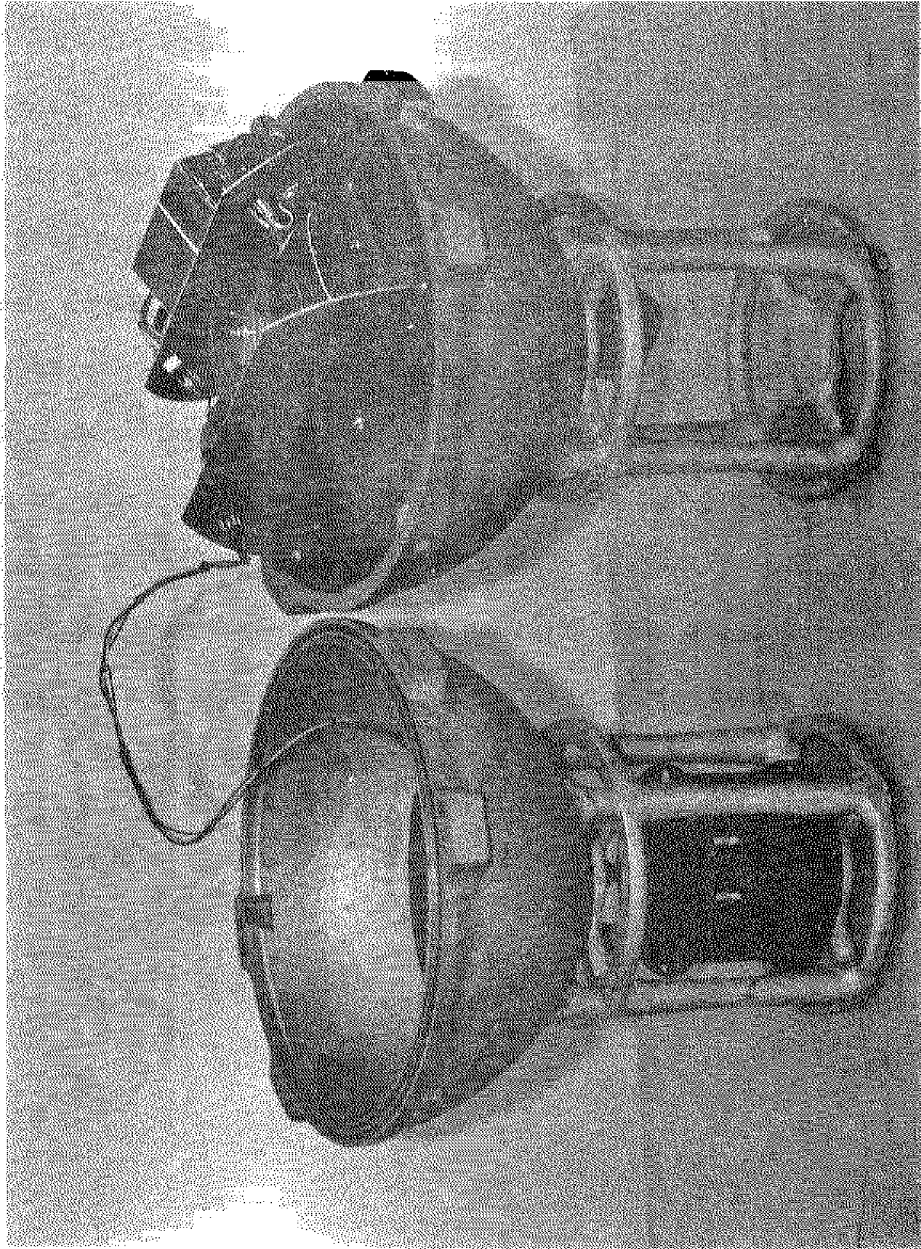


Figure 16. Spherical instrument package.

speed sensor is protected by one birdcage and the pressure, temperature, and conductivity sensors by the other cage.

The new spherical instrument package, in conjunction with the new roller block, buoyancy control mechanism, and plastic fairing, offer several improvements over the original vertical profiler. The repackaged sphere weighs significantly less than the cylindrical package and is almost neutrally buoyant. The new profiler thus produces less drag force at the roller block and allows small displacement changes in the buoyancy control mechanism to regulate the profiler's ascent and descent. Being located forward of the plastic housing and the mooring cable, the sensors sample undisturbed water. The horizontal orientation of the axis of the rotor in the profiler's pitch axis offers a distinct improvement in rotor accuracy. The most important feature of the new profiling system is its ability to profile continuously in an unattended mode.

CHAPTER V
INCLINOMETER

A single-axis inclinometer that measures angular displacement of the spherical pressure housing with respect to the local vertical (gravity vector) has been designed and constructed. Because of the critical lack of unutilized space in the sphere and the rigid buoyancy constraints on instrument package density, the inclinometer was designed under close size and weight specifications.

The inclinometer, as designed, satisfies the following specific requirements:

1. The mechanical angle measured is 90° ($\pm 45^{\circ}$).
2. The electrical output, to be compatible with the data logger, is in the form of a resistance reading with a range between 0 and 2,500 ohms.
3. The maximum weight of the instrument is 4 ounces.
4. The maximum dimensions allow the instrument to fit into a spherical segment of the 10 inch pressure vessel with a 9 inch cord height.
5. The instrument's resistance output reading does not vary significantly with temperature variations.
6. Angular displacement resolution is within one degree.

Two types of transducers were investigated in the study. The first utilized the principle of a liquid level indicator. A resistance wire was inserted into a circular plastic tube that was half filled with mercury. The two ends of the plastic tube were sealed together and the

circular tube formed a toroid. Another wire was inserted through a small hole in the tubing at the nadir of the semi-circular mercury column and makes electrical contact with the mercury. As the plastic tube is rotated through an angular displacement, the mercury remains in the bottom half of the toroid and shorts out a segment of the resistance wire proportional to the angular displacement.

To meet the imposed design specifications, a 28 inch length of 0.5 inch ID, 0.75 inch OD plastic tubing was selected. Triple distilled instrument grade mercury half filled the toroid. The upper half of the tube was filled with 200 centistoke silicone oil (200 centistokes at 25°C). The silicone oil damped out unwanted oscillations of the mercury and reduced the cohesive effect between the mercury and the resistance wire. A 0.25 inch acrylic rod was threaded to 100 threads/inch and 36 gauge Chromel-A (80% Ni, 20%Cr) resistance wire was laid in the threads. The acrylic rod, with the resistance wire held securely in place, was heated with a hot air gun and bent to conform to the radius of the toroid.

The mercury transducer was displaced from the vertical at 10 degree increments and the resistance readings were recorded over a range of -40 to +40 degrees. A least squares regression analysis was performed on the data to determine the calibration equation. As predicted, the resistance output and angular displacement were highly correlated ($r = 0.99$). In the linear regression equation $Y = b_0 + b_1X$ (Y in ohms and X in degrees), $b_0 = 389.0$ and $b_1 = -5.4$. The standard error of estimate, a measure of the average discrepancy between the observations and the fitted line, was 18.6.

Two serious problems prevented the use of this device. First, the

36 gauge Chromel-A wire had a resistance to length ratio of 25 ohms/foot. The maximum number of threads per inch that could be machined on the plastic rod was 100. Therefore, the maximum resistance (in ohms) per circumference inch was 156, about half of the required 286. This problem could have been corrected with a smaller gauge wire but a more significant problem forced the abandonment of the Hg-resistance wire approach. After twenty-four hours of contact between the mercury and the Chromel-A wire, an amalgamation formed in the mercury. This contaminate clung to the turns of the wire as the toroid was displaced angularly and shorted out additional turns of wire which resulted in an erroneous relationship between resistance and angular displacement. Pigeon and Denner (1968) used a platinum resistance wire in a mercury filled capillary in a resistance tide gauge and obtained excellent results. While having an acceptable coefficient of thermal expansion ($8.0 \times 10^{-5} \text{ C}^{-1}$) and temperature coefficient of resistance ($2.5 \times 10^{-5} \text{ C}^{-1}$), the resistivity of the platinum wire is only 6.5 ohms/foot, about one fourth the resistivity of Chromel-A wire.

A single-axis pendulous (gravity referenced) potentiometer was selected for the angular displacement sensor. The relatively simple instrument is essentially a plumb bob with a resistance output. Figure 17 illustrates a typical configuration for a single-axis pendulous sensor and defines the symbols used in the dynamic analysis. The desired input to be measured is the case rotation angle θ_c . Doebelin (1966) makes the following simplifying assumptions in his analysis of the problem.

1. Angles are small enough so that the sine and the angle are nearly equal and the cosine is nearly one.

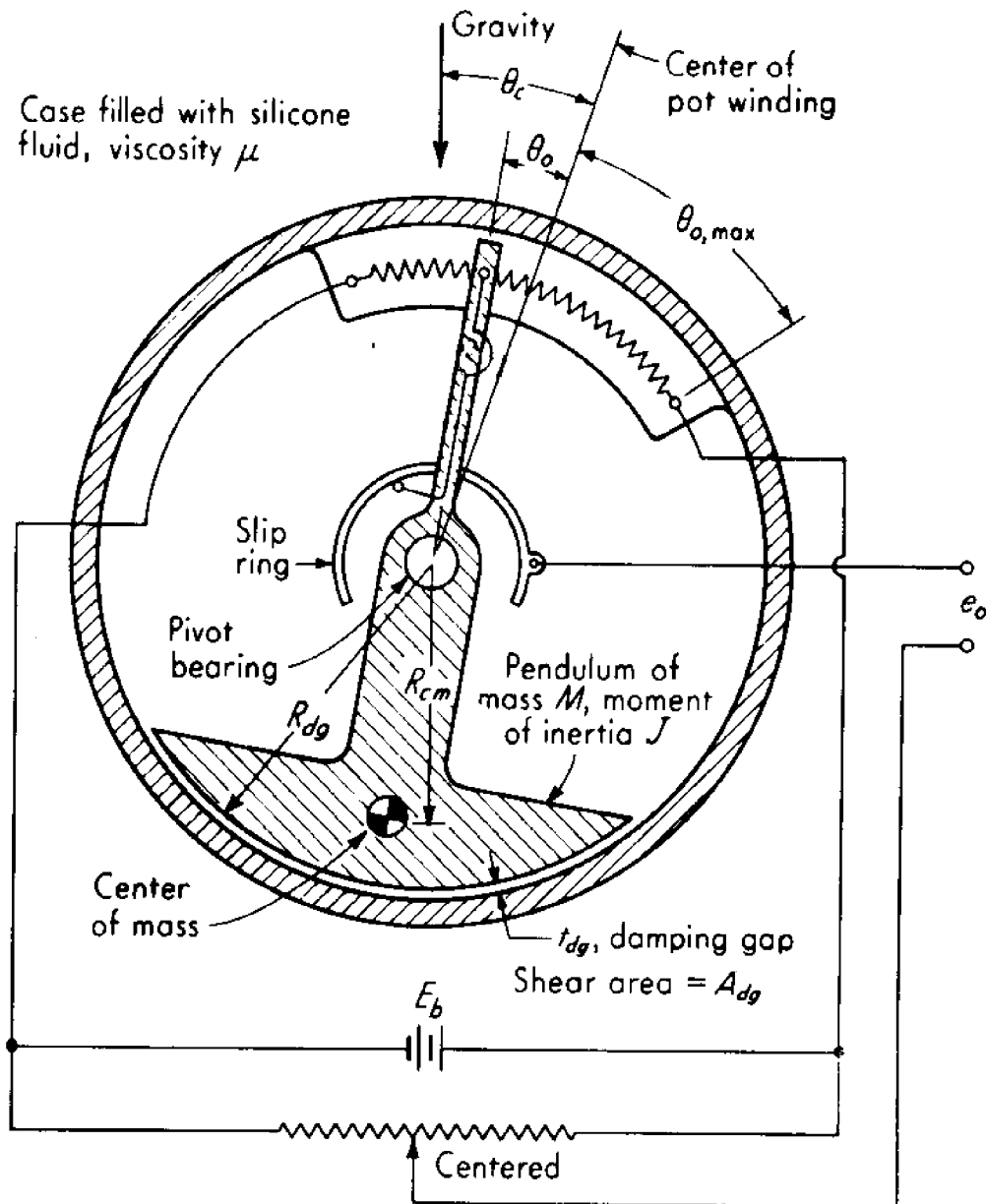


Figure 17. Pendulum displacement sensor.

2. The inertial effect of the fluid on the pendulum motion is negligible.

3. The damping effect of the fluid is limited to the damping gap.

4. All dry friction effects of pots and wipers, bearings, and slip rings may be neglected for dynamic analysis.

5. The buoyant force on the pendulum is negligible.

The result of Doebelin's analysis is:

$$\frac{e_o}{\theta_c} (D) = \frac{K_e (D^2/\omega_n^2 + 1)}{D^2/\omega_n^2 + 2\zeta D/\omega_n + 1}$$

where

$$\omega_n = \sqrt{\frac{Mg R_{cm}}{J}}$$

$$\zeta = \frac{B}{2\sqrt{JMg R_{cm}}}$$

$$B = \frac{R_{dg}^2 \mu A_{dg}}{t_{dg}}$$

$$K_e = \frac{E_b}{2\theta_{o,max}}$$

$$D = \frac{d}{dt}$$

Figure 18 shows an exploded view of the designed sensor. The plastic housing was machined from 0.125 inch plexiglass. All metallic parts, except the stainless steel shaft of the potentiometer, are either aluminum or brass to minimize interference with the magnetic compass in the sphere.

The potentiometer selected was the Model 85111 Microtorque manufactured by the Instrument/Controls Division of the Conrac Corporation. This single-turn precision potentiometer has jewel bearings and a precious metal winding. The mechanical and electrical specifications are summarized

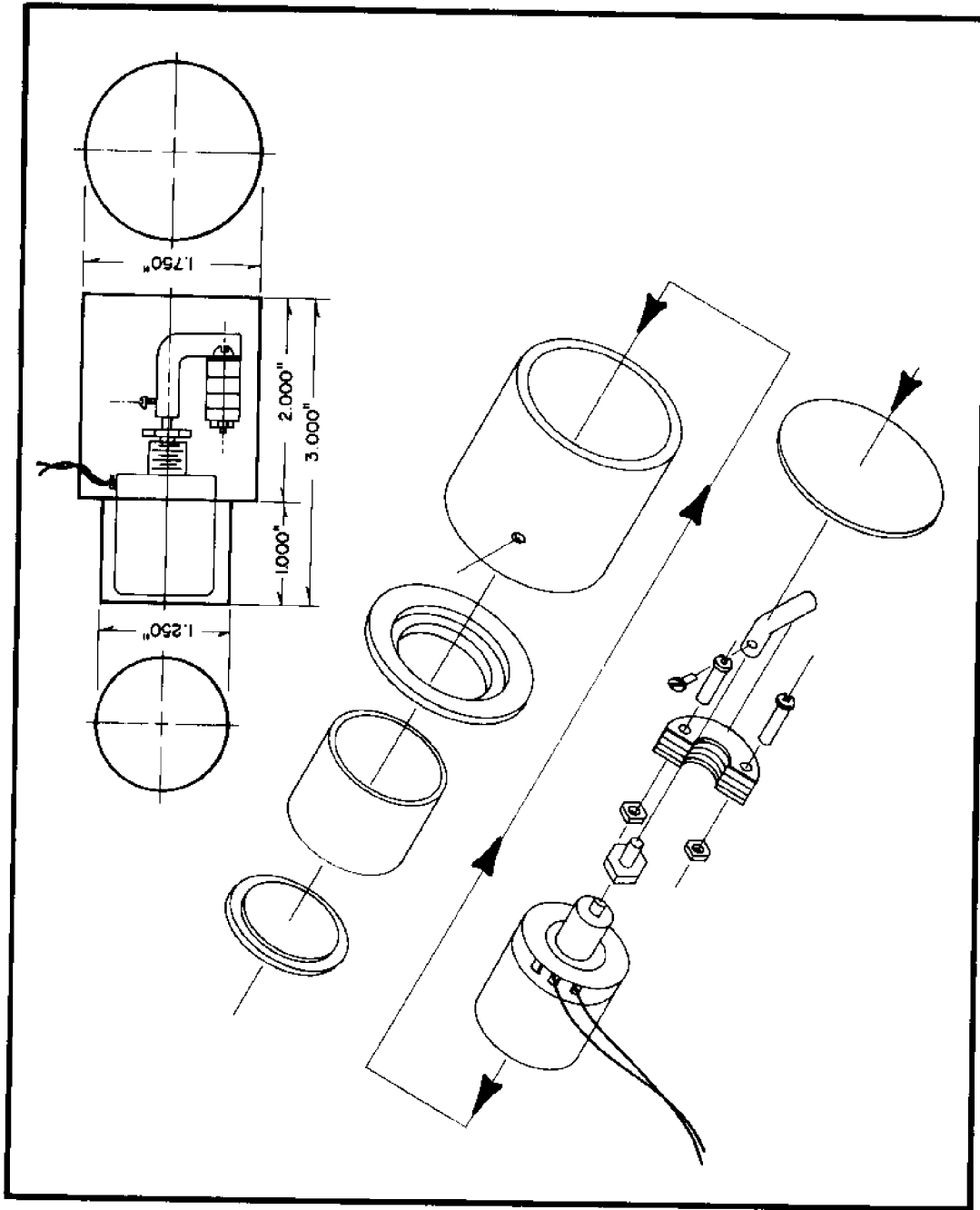


Figure 18. Exploded view of inclinometer.

below:

1. Operating torque: 0.006 inch-ounces (maximum).
2. Shaft diameter: 0.031 inch.
3. Weight: 0.6 ounce.
4. Coil resistance: 0-10,000 ohms.
5. Resistance tolerance: $\pm 5\%$.
6. Temperature coefficient of resistance: 240 ppm.
7. Linearity tolerance: $\pm 0.5\%$.

Hysteresis and oscillatory errors were minimized with the following design values:

$$t_{dg} = 0.0625 \text{ inch}$$

$$R_{dg} = 0.6875 \text{ inch}$$

$$R_{cm} = 0.5 \text{ inch}$$

$$M = 0.5 \text{ ounce}$$

$$\mu = 200 \text{ centistokes (at } 25^{\circ}\text{C)}$$

$$\theta_0, \text{ max} = 45 \text{ degrees}$$

The pendulum sensor is sensitive to horizontal accelerations. When exposed to a vibration test of 0.125 inch amplitude and frequencies between 0.25 and 10 Hz, the maximum error introduced was 50 ohms (2 degrees).

The pendulous potentiometer was displaced from the vertical at 10 degree increments and the resistance readings were recorded for calibration analysis. A least squares regression analysis was performed on the data to determine the calibration equation. As is the case with the mercury transducer, the resistance output and angular displacement were highly correlated ($r = 0.99$). In the linear regression equation $Y = b_0 + b_1 X$ (Y in ohms and X in degrees), $b_0 = 1458.7$ and $b_1 = 33.2$.

The standard error of estimate was 73.0.

Figure 19 shows the positioning of the inclinometer in its spherical pressure housing.

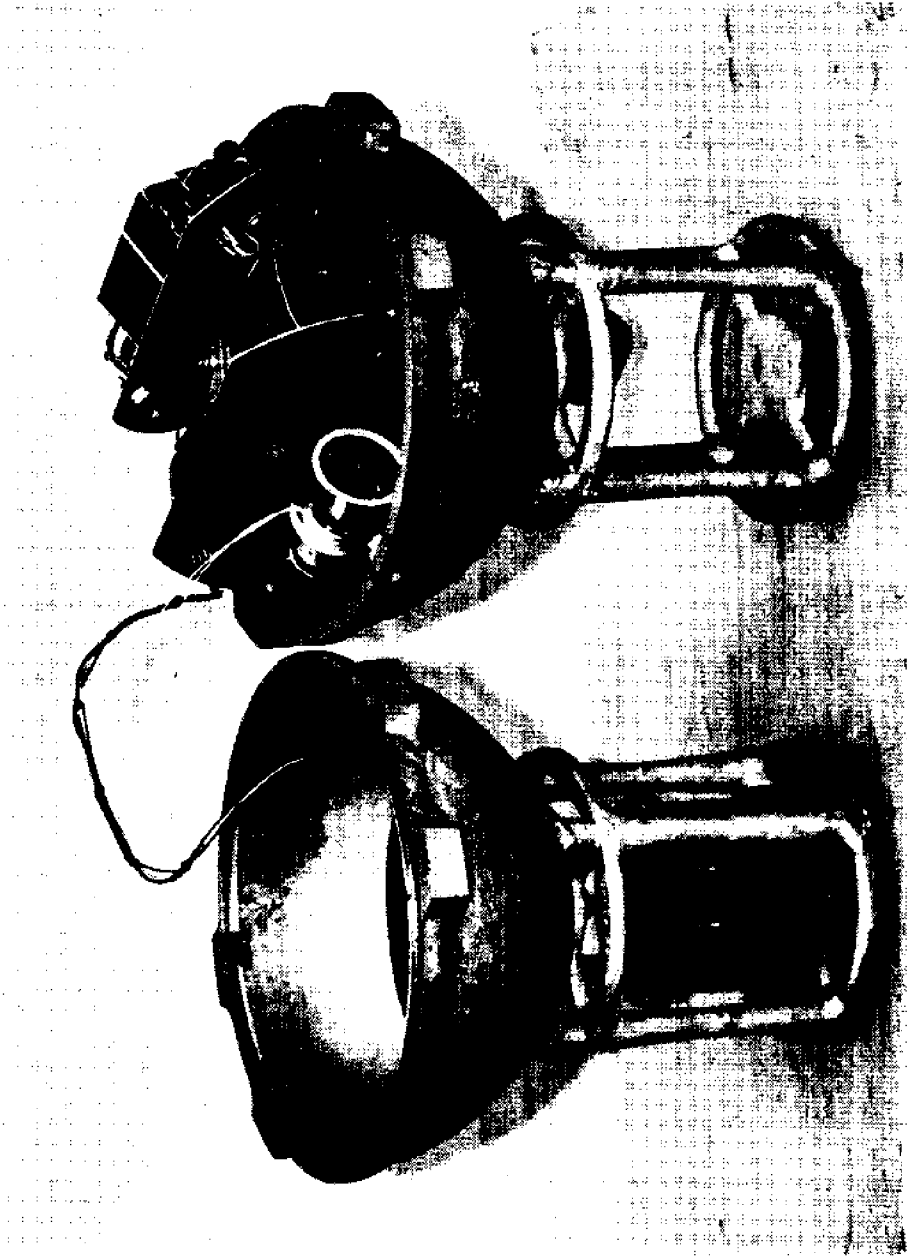


Figure 19. Inclinometer in spherical instrument package.

CHAPTER VI
DATA SUMMARY AND ANALYSIS

The rotor gear train reduces the rotational rate of the rotor to a speed acceptable for driving the current measuring potentiometer. This potentiometer has been designed to rotate continuously with a negligible dead angle. Thus the potentiometer presents the value in an integrated form which is particularly advantageous in that the average current speed can be calculated even if one or more data measurements are unreadable or lost. The current speed readings will appear on the magnetic tape, and therefore, the print-out, as progressively decreasing numbers, beginning at 1023 everytime the potentiometer passes the dead zone, and ending at zero as the potentiometer enters the dead zone.

Table 1 shows the data format selected for this experiment's print-out. The progressive decimal numbers are read from left to right and down the page. Because the only parameter sampled in this study was current speed, each column contains current speed measurements only. In the normal mode of operation, where five parameters plus a reference number are sampled, the data are printed in six columns and there is one column for each of the six channels of the instrument. In the normal mode, the printer adds the line number which will also be the number for the progressive measurements on the tape.

To modify the data logger to measure and record current speed only, the L-shaped pin at the periphery of the rotating cover plate of the en-

Table 1
Data Format of Current Velocity Measurement Print-Out

Tape File No. 3	Block No. 23					
463	994	994	994	994	994	994
464	994	994	994	994	994	994
465	994	994	994	994	994	994
466	994	994	994	994	994	994
467	994	994	994	994	994	994
468	994	994	994	994	994	994
469	994	994	994	994	994	994
470	994	994	994	994**	992	988
471	984	981	977	974	970	966
472	962	958	955	951	948	943
473	941	938	934	930	927	923
474	920	915	910	905	901	897
475	893	889	884	879	873	869
476	865	860	857	854	848	843
477	839	834	830	826	822	817
478	813	808	804	800	796	792
479	787	783	779	773	770	765
480	760***	759	759	759	759	759
481	759	759	759	759	759	759
482	759	759	759	759	759	759
483	750	759	759	759	759	759

** rotor untied

*** rotor tied

coder had to be removed. The removal of this pin disabled the selector switch from rotating and the current speed channel (number six) was read and recorded at every sampling interval. The rotor was tied for about five minutes each time the test fixture was inclined and the tripod was adjusted between measurements. The constant readings in table 1 reflect the period of time at which the rotor was secured.

To calculate the current speed from a set of current measurements consisting of successively decreasing numbers, the incremental difference between successive numbers must be obtained. With this difference, the gear train reduction ratio (1200:1 in this experiment), and the fact that 1024 potentiometer units equal 357 degrees, one obtains the number of revolutions of the rotor during the sampling interval. With the length of the sampling interval known (5 seconds in this experiment), it is possible to calculate the average rotor speed in revolutions per minute. The average current speed during the sampling interval can then be read from the rotor calibration curve, given in the instrument's technical operating manual.

When the reading of the instrument is 1023 or zero, the potentiometer is in the dead zone and its true position is unknown. When in the dead zone, the current speed cannot be calculated and these readings should not be used. But it is possible to calculate the average current speed during the time the potentiometer travels through this zone. Since the dead angle is approximately 3 degrees, it follows that the dead-angle zone corresponds to

$$\frac{3}{360-3} \times \frac{1024}{1} = 9 \text{ units}$$

and that a full rotation of the current measuring potentiometer corres-

ponds to 1033 units (Aanderaa, 1967).

Tables 2 and 3 present a summary of the data collected with the cylindrical and spherical instrument packages at different positions of tilt. The data are presented in the following format.

1. Inclination - the angle of attack of the horizontal current with respect to the vertical axis of the rotor.
2. Observations - the number of readings taken at each position of inclination.
3. Mean - the average of the incremental change in the current measuring potentiometer readings within the 5 second sampling interval.
4. Standard deviation - the root mean square of the deviations about the mean.
5. Standard error of the mean - the standard deviation of the sampling distribution of the mean.
6. Ratio - the ratio of the rotor rotation rate at the position of inclination to the rotor rotation rate in the vertical position.

Savonius rotor tilt correction tables and graphs are given in the oceanographic literature. Sundblad (1965) presented the following tilt correction table for the Type 316 Histogram Current Meter manufactured by the Braincon Corporation, Marion, Massachusetts.

ROTOR INCLINATION FROM VERTICAL	
Angle	Error
5°	3%
10°	6%
20°	12%
30°	20%

Note that Sundblad's table suggests that the error is independent of

Table 2
Summarized Data From Inclination of Cylindrical Instrument Package

Inclination	Observations	Mean	Standard Deviation	Standard Error	Ratio
0°	67	3.687	0.58	0.07	1.000
-11°	68	3.471	0.63	0.08	0.941
-22°	68	3.103	0.72	0.09	0.842
-33°	66	1.970	0.63	0.08	0.534
+11°	63	3.540	0.67	0.08	0.960
+22°	68	3.059	0.71	0.09	0.830
+33°	68	2.177	0.65	0.08	0.590

Table 3
Summarized Data From Inclination of Spherical Instrument Package

Inclination	Observations	Mean	Standard Deviation	Standard Error	Ratio
0°	56	4.143	0.84	0.11	1.000
-11°	58	4.345	0.89	0.12	1.049
-22°	58	4.276	1.15	0.15	1.032
-33°	58	3.569	0.65	0.09	0.862
+11°	57	2.667	0.69	0.09	0.644
+22°	60	3.083	0.87	0.11	0.744
+33°	58	2.190	0.85	0.11	0.529

the direction of tilt and will result in a lower than true reading in every case. No current speed range was given for which these correction factors apply.

Richardson, Stimson, and Wilkins (1963) presented the following tilt correction table for the recording current meters they used in moored buoy stations between December 1960 and April 1963.

ROTOR INCLINATION FROM VERTICAL Angle	Error
15°	10%
20°	15%
30°	25%
45°	65%

Richardson states that all tilt errors cause the instrument to read low. This table, as in the case with Sundblad's table, suggests that the error is independent of the direction of tilt. No current speed range was given for which these correction factors apply.

Gaul (1963) evaluated the effect of tilt on 3 rotors with housings and one rotor without a housing. Figure 20 shows the results obtained by Gaul with the unhoused rotor. The graph of the same rotor in a housing (not shown in this paper) shows a larger tilt error at every angle of inclination. The curve of the unhoused rotor was selected for comparison in this study because it represents the most conservative case. Gaul's study points out four significant characteristics of the Savonius rotor not shown in the two preceding tables:

1. The induced error is not independent of the direction of tilt.
2. The rotor housing has a definite effect on the magnitude of the induced error.

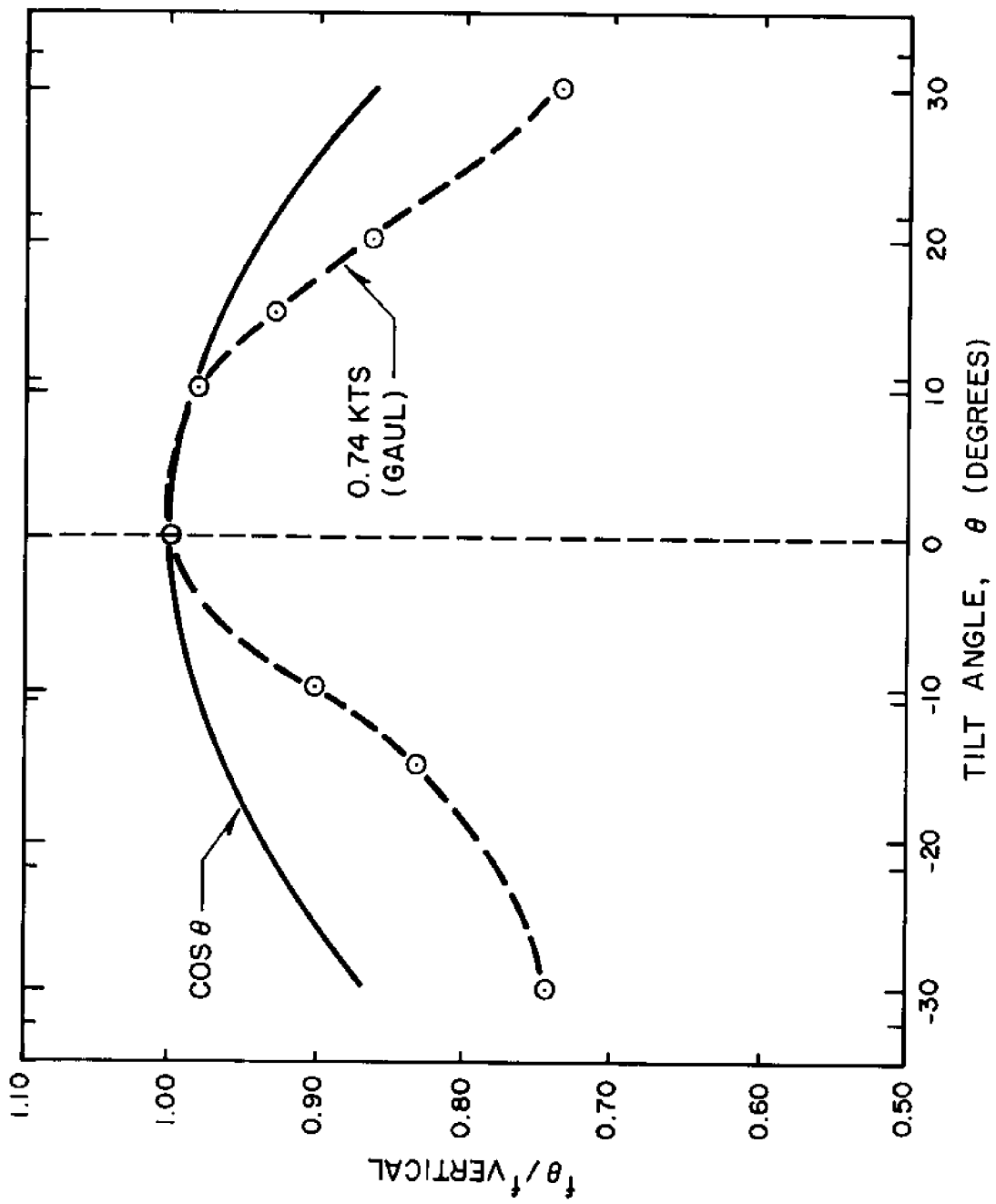


Figure 20. Influence of tilt on rotor output.

3. The induced error does not always cause the rotor to rotate at a slower rate.

4. The same rotor will have different magnitudes of induced error in flows of different velocity.

The cosine curve is included in figure 20 and shows the disagreement between the cosine error curve assumption and the true error curve. Many oceanographic instrumentation manufacturers today state that their Savonius rotor current meters follow the cosine error curve for tilt corrections (Hydro Products, 1972).

Figure 21 displays graphically the information summarized in table 2. A slight degree of asymmetry can be distinguished in the curve. A definite correlation exists between the rotation rate ratio and the angle of tilt. The correlation coefficient is $r = 0.93$ for the negative angles and $r = 0.95$ for the positive angles. Figure 21 shows a definite departure by the relative rotation rate curve from the cosine curve, especially at angles larger than 10 degrees.

Figure 22 displays graphically the information summarized in table 3. The author considers the effects shown in figure 22 to be the most significant feature of this study. At first glance, one would be inclined to say that the data point at +11 degrees represents bad data and should have a value around 0.85 versus 0.64. As summarized in table 3, the 0.64 value is based upon 57 observations, taken at 5 second intervals, with a standard error of the mean equal to 0.09.

The birdcage on the spherical instrument package has unusually large struts. The cylindrical struts are slightly hourglass shaped with the strut diameter at the tops and bottoms being 0.75 inch and the strut diameter at the midpoint being 0.50 inch. The rotor is located 1.0 inch

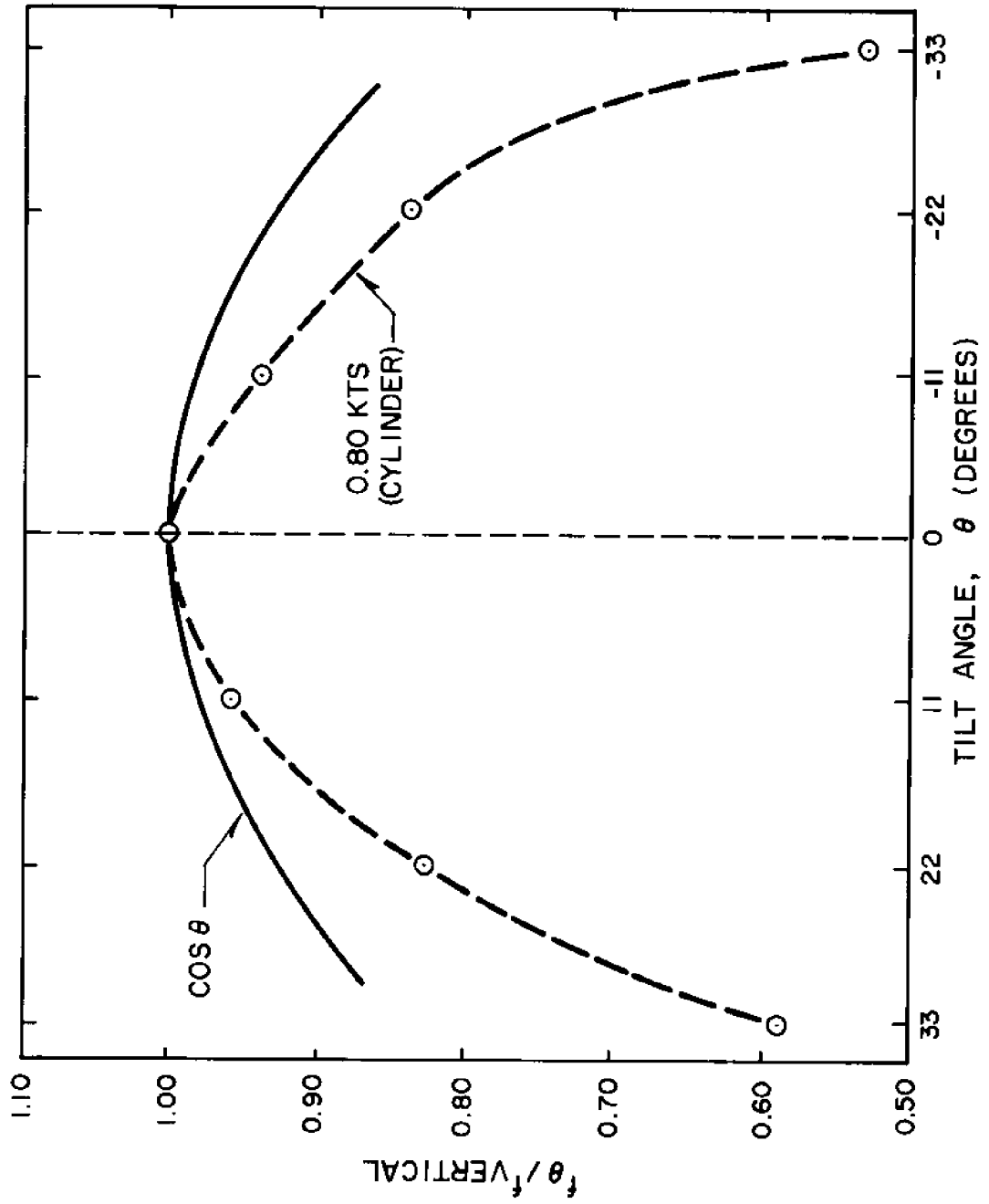


Figure 21. Influence of tilt on cylindrical instrument package.

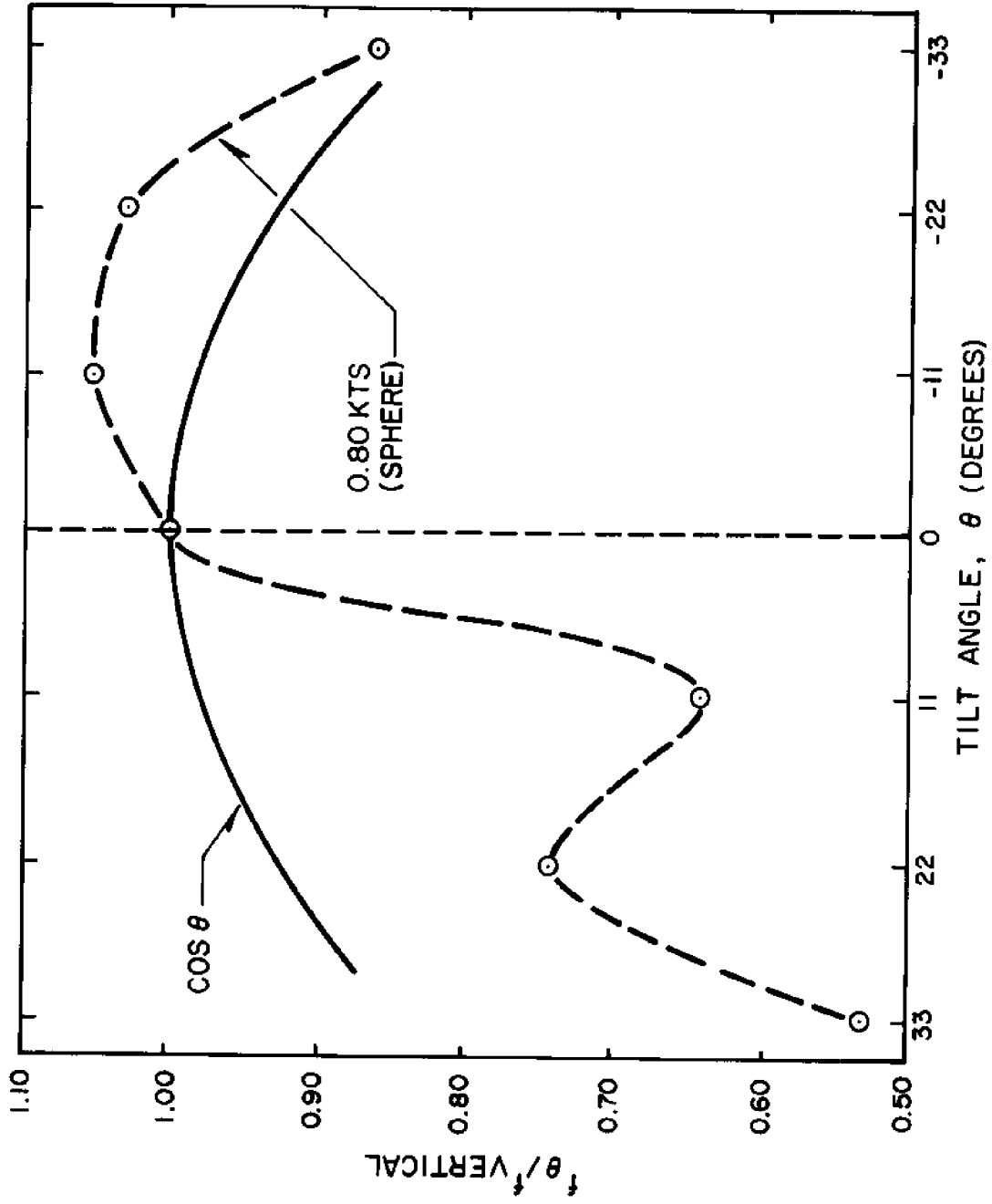


Figure 22. Influence of tilt on spherical instrument package.

below the top strut circle and 2.25 inches above the lower strut circle. While it protects the rotor from physical damage, the birdcage interacts with the turbulent current flow and creates different flow regimes at different angles of inclination. The spherical pressure vessel might also play a significant role in the complex turbulence generation and energy absorption phenomena associated with the birdcage rotor housing. At +11 degrees, the wake and modified flow tend to stall out the rotor while at -11 and -22 degrees, the rotor rotation rate increases. Gaul (1963) and Sexton (1964) both observed an increase in relative rotation rate when certain rotors are tilted in one preferential direction. But a search of the literature has not revealed a dip occurring in the relative rotation rate curve. Further investigations need to be conducted to determine if this dip is a result of just the birdcage flow path interactions, and would have also occurred in tow tank experiments, or if this dip is a result of the scale of turbulence involved in this study. If the latter proves to be the case, all previous tilt correction graphs and tables obtained in tow tank experiments will need to be re-evaluated in a turbulent flow regime similar to that experienced during in situ data collection. This will also necessitate a critical review of the theories and phenomenological descriptions generated from the analysis of that data.

Correlation coefficients were calculated on the data presented in figure 22 to measure the correlation between the rotation rate ratio and the angle of tilt. The correlation coefficient is $r = 0.66$ for the negative angles and $r = 0.84$ for the positive angles.

A statistical analysis was performed on the data shown in figures 21 and 22 to determine if there is a statistically significant difference

between the relative rotation rate curves and the cosine curve. In each case, the null and alternative hypotheses were as follows:

H_0 : The relative rotation rate curve and the cosine curve produce, on the average, the same tilt correction factor ($u_D = 0$).

H_a : The relative rotation rate curve and the cosine curve do not produce, on the average, the same tilt correction factor ($u_D \neq 0$).

The null hypothesis will be accepted or rejected based on the $p = 0.20$ level of significance value. Because figures 21 and 22 show an obvious departure from the cosine curve, the author took the liberty of adopting a conservative approach to the two-tailed t-test which greatly reduced the total number of calculations involved. Instead of incorporating every observed value at each angle of tilt, only the mean value of the observations were considered. This conservative approach reduced the degrees of freedom from over 200 to 3. The results are summarized below:

1. Spherical instrument package and positive tilt angles:

$$S_{\bar{D}} = .32 \qquad df = 3 \qquad t = 2.70$$

result: reject the null, accept the alternative hypothesis

2. Spherical instrument package and negative tilt angles:

$$S_{\bar{D}} = .10 \qquad df = 3 \qquad t = 2.09$$

result: reject the null, accept the alternative hypothesis

3. Cylindrical instrument package and positive tilt angles:

$$S_{\bar{D}} = .21 \qquad df = 3 \qquad t = 1.63$$

result: reject the null, accept the alternative hypothesis

4. Cylindrical instrument package and negative tilt angles:

$$S_{\bar{D}} = .25 \qquad df = 3 \qquad t = 1.58$$

result: accept the null hypothesis

While the null hypothesis was accepted in case 4, an increase of one degree of freedom ($df = 4$) would have resulted in a rejection of the null hypothesis and an acceptance of the alternative hypothesis.

Figure 23 presents a comparison between the relative rotation rate curves of the cylindrical and spherical instrument packages. Figures 24 and 25 compare the two instrument packages with the un-housed rotor studied by Gaul (1963).

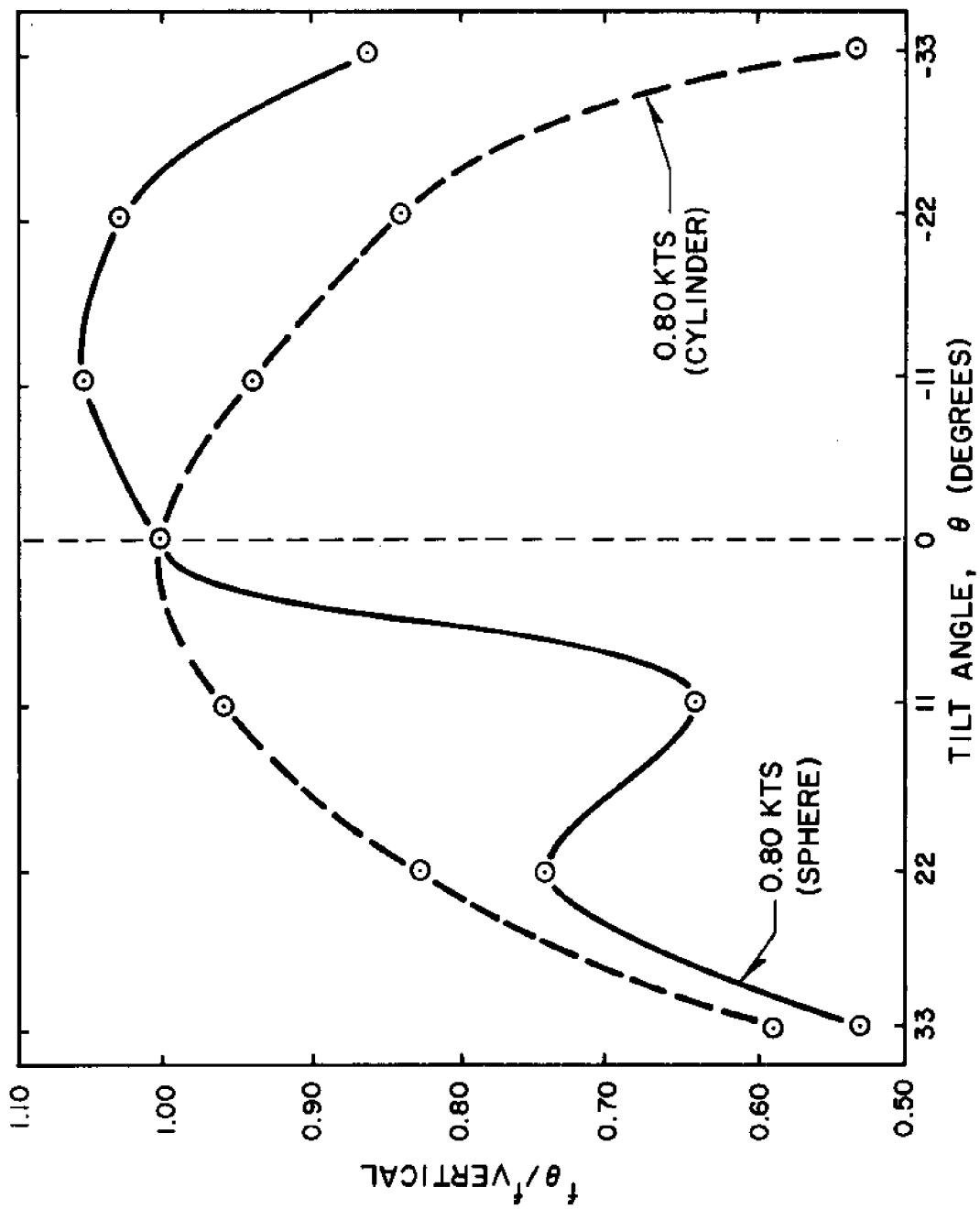


Figure 23. Influence of tilt on cylindrical and spherical instrument packages.

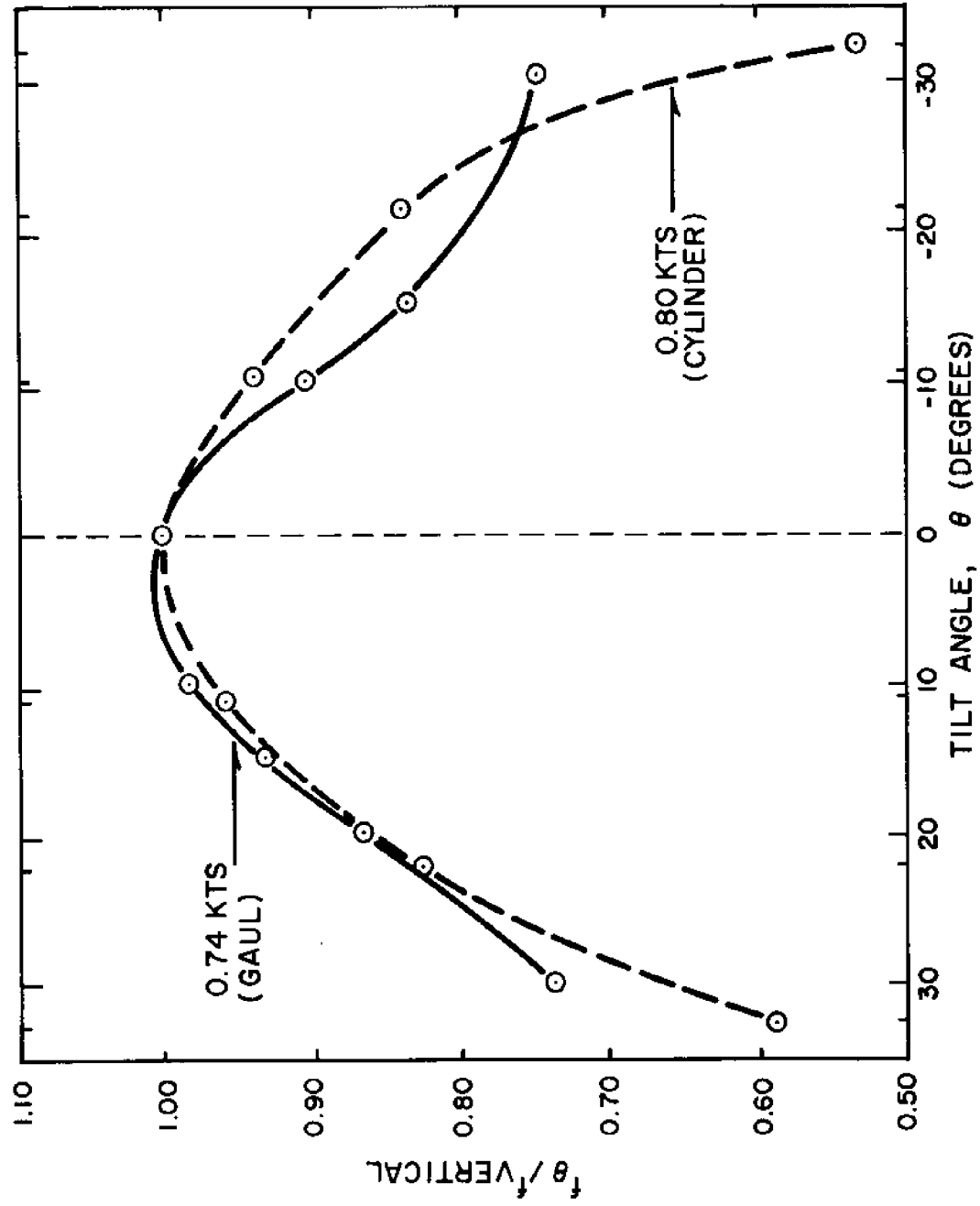


Figure 24. Comparison of unhoused rotor and cylindrical instrument package.

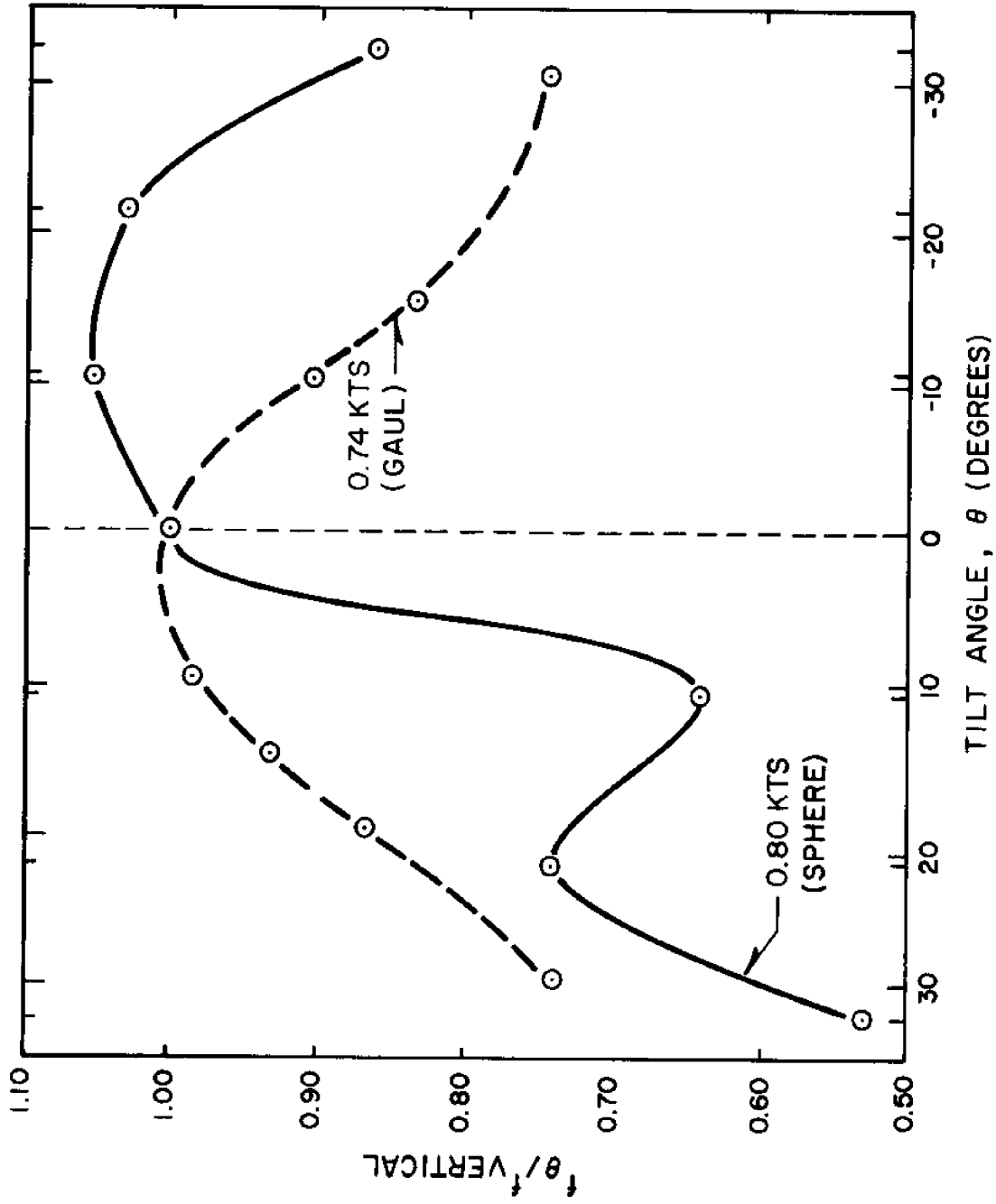


Figure 25. Comparison of unhoused rotor and spherical instrument package.

CHAPTER VII

CONCLUSIONS AND RECOMMENDATIONS

This study was undertaken to observe the effects of tilt on a Savonius rotor exposed to a turbulent flow regime. Four specific objectives were established to achieve this end. The objectives were:

1. Determine and plot the curve of relative rotation ratio versus angle of tilt (in a turbulent horizontal flow pattern) for the Aanderaa model 4 current meter used by Düing and Johnson in their high resolution current profiling experiments in the Straits of Florida (Düing and Johnson, 1972).
2. Determine and plot the curve of relative rotation ratio versus angle of tilt (in a turbulent horizontal flow pattern) for the repackaged recording current meter presently in use by Van Leer and Düing in their unattended profiling system (Van Leer and Düing, 1972).
3. Compare the data collected in this study with the observations obtained by other investigators analyzing the effects of tilt on a Savonius rotor exposed to a non-turbulent (or turbulent suppressed) flow regime.
4. Develop an instrument to detect the occurrence, magnitude, and direction of rotor inclination.

Figure 21 is a plot of the relative rotation ratio versus angle of tilt for the Aanderaa model 4 current meter. The curve is asymmetrical and significantly departs from the cosine curve for both positive and negative directions of tilt. A decrease in relative rotation ratio is

observed with increasing positive and negative angles of tilt. Figure 24 presents a comparison between this rotor configuration and the rotor studied by Gaul (1963). Close agreement is shown between the curves for the angular range -5 to +22 degrees but rapid divergence occurs at the larger angles of tilt.

Figure 22 is a plot of the relative rotation rate versus angle of tilt for the repackaged recording current meter. The curve is asymmetrical and significantly departs from the cosine curve for both positive and negative directions of tilt. As the rotor was inclined in the positive direction, a rapid decrease in relative rotation ratio was observed at +11 degrees, followed by an increase at +22 degrees, and a further decrease at +33 degrees. When the rotor was inclined in the negative direction, an increase in relative rotation rate was observed at -11 and -22 degrees, followed by a decrease at -33 degrees. Figure 25 presents a comparison between this rotor configuration and the rotor studied by Gaul (1963). A large divergence is observed at all angles of tilt.

Figure 23 presents a comparison of the Aanderaa rotor in two different pressure vessel and rotor housings. Significant disagreement is observed at most angles of inclination. There appears to be some convergence at large positive angles.

The following list summarizes the rotor response characteristics that were mutually observed during this study and the investigations performed by Gaul (1963), Hankins (1963), Richardson (1963), Sexton (1964), and Sundblad (1965).

1. The output of a Savonius rotor is dependent upon the angle of attack between the axis of the rotor and the axis of the current flow.

2. The output of a Savonius rotor is dependent upon the direction of tilt relative to the current flow.

3. The output of a Savonius rotor does not always decrease with increasing angles of tilt.

4. The output of a Savonius rotor is dependent upon the size and configuration of the rotor housing appurtenances and the instrument case.

5. The output of a Savonius rotor as it is inclined from the vertical deviates significantly from a dependency on the cosine of the angle of tilt.

The author considers the two major limitations in this study to be: (1) the Aanderaa rotor is not a "true" Savonius rotor, and (2) the instrument pressure vessels did not experience uniform velocity profiles.

The Aanderaa single tier rotor is 2.75 inches high and has a rotor diameter of 4.125 inches. The rotor utilizes six 1.25 inch diameter half cylinder vanes in the configuration shown in figure 19. The similarity between the two curves shown in figure 24 indicates the validity in comparing their rotor output responses to inclination.

Within the accuracy of the Bendix ducted current meter, the rotor was exposed to a uniform velocity profile. But as discussed in the experimental design, the pressure housings did not experience a uniform velocity profile. If the housings do play a role in the flow pattern modification, this study looked at the conservative condition. The author feels that the deviations observed in figure 22 would be accentuated due to the streamline concentrating effect of the sphere, if a uniform velocity profile was felt by rotor and pressure housing.

The experimental limitations imposed by time and facilities prevented

the author from investigating many aspects of this study. The following recommendations for further investigation are suggested:

1. The spherical and cylindrical instrument packages should be inclined in a non-turbulent tow tank at the same speed (0.80 knots) as this experiment. These data would assist in distinguishing the exact role of turbulence and possibly explain the dip shown in Figure 22.
2. This same experiment should be conducted at various current speeds. Gaul (1963) and Sexton (1964) observed different rotor output ratios for the same angles of tilt at different current speeds.
3. This same experiment should be conducted under various scales of turbulence.
4. A dye study should be performed to identify the flow patterns around the rotor.
5. The spherical instrument package, with a rotor guard similar to that of the cylindrical instrument package, should be retested. If an improved rotor error curve results, the present birdcage should be eliminated and replaced with the rotor guard.

BIBLIOGRAPHY

1. Aanderaa, I. R., A Recording and Telemetering Instrument, Tech. Rept. NATO Subcom. Oceanogr. Research, 16(46), 1964.
2. Aanderaa, I. R., Operating Manual for Recording Current Meter. Nesttun, 1967.
3. Almeida, J. M., Aanderaa to Digital Magnetic Tape Conversion System, 1972. (Report in preparation).
4. Dahl, O., "The Capability of the Aanderaa Recording and Telemetering Instrument," Progress in Oceanogr., 5: 103-106, 1969.
5. Doebelin, E. O., Measurement Systems: Application and Design. New York: McGraw-Hill Book Company, 1966.
6. Düing, W., and Johnson, D., "High Resolution Current Profiling in the Straits of Florida," Deep-Sea Research, 19: 259-274, 1972.
7. Fofonoff, N. P., and Ercan, Y., Response Characteristics of a Savonius Rotor Current Meter, Woods Hole Oceanographic Institution, Tech. Rept. 67-33, 1967. Unpublished.
8. Forstall, W., and Gaylord, E. W., "Momentum and Mass Transfer in a Submerged Water Jet," Journal of Applied Mechanics, pp. 161-164, June 1955.
9. Gaul, R. D., Instrumentation and Data Handling System for Environmental Studies off Panama City, Florida, Department of Oceanography and Meteorology, A & M College of Texas, Tech. Rept. 62-1T, 1962a. Unpublished.
10. Gaul, R. D., The Savonius Rotor Current Meter, Department of Oceanography and Meteorology, A & M College of Texas, Tech. Rept. 62-2T, 1962b. Unpublished.
11. Gaul, R. D., Influence of Vertical Motion on the Savonius Rotor Current Meter, Department of Oceanography and Meteorology, A & M College of Texas, Tech. Rept. 63-4T, 1963. Unpublished.
12. Gaul, R. D., Snodgrass, J. M., and Cretzler, D. J., Some Dynamical Properties of the Savonius Rotor Current Meter, ISA Marine Sciences Instrumentation, 2, 1963.
13. Hankins, T. L., Report on the Performance of the Savonius Rotor, Geodyne Corporation, Waltham, Massachusetts, 1963. Unpublished.

14. Hinze, J. O., Turbulence. New York: McGraw-Hill Book Company, 1959.
15. Hydro Products, Personal communication, 1972.
16. Maury, M. F., The Physical Geography of the Sea. Harper and Brothers, 1858.
17. Paquette, R. G., Practical Problems in the Direct Measurement of Ocean Currents, ISA Marine Sciences Instrumentation, 2, 1963.
18. Pigeon, N. B., and Denner, W. W., A Resistance Tide Gauge, ISA Marine Sciences Instrumentation, 4, 1968.
19. Richardson, W. S., Instruction Manual for Recording Current Meter, Woods Hole Oceanographic Institution, Tech. Rept. 62-6, 1962. Unpublished.
20. Richardson, W. S., Stimson, P. B., and Wilkins, C. H., "Current Measurements from Moored Buoys," Deep-Sea Research, 10: 369-388, 1963.
21. Savonius, S. J., The Wing-Rotor in Theory and Practice. Finland: Savonius and Company, 1925.
22. Savonius, S. J., "The Savonius Rotor and its Applications," Mechanical Engineering, 53(5): 333-338, 1931.
23. Sexton, R., Some Tow Tank Calibrations of the Savonius Rotor, Lamont Geological Observatory, Columbia University, Tech. Rept. Cu-11-64, 1964. Unpublished.
24. Shearer, J. J., A Decoding Interface for the Aanderaa or Plessey Current Meter, Rosenstiel School of Marine and Atmospheric Science, University of Miami, 1972.
25. Shepherd, D. G., Elements of Fluid Mechanics. New York: Harcourt, Brace, and World, Inc., 1965.
26. Snodgrass, J. M., Prototype Telemetering Current Sensor, Scripps Institution of Oceanography, Tech. Rept. 55-10, 1955. Unpublished.
27. Sundblad, R. L., The Histogram Current Meter, ISA Marine Sciences Instrumentation, 3, 1965.
28. Van Leer, J., and Düing, W., Personal communication, 1972. (Report in preparation).

